ERDC/ITL TR-23-1

US Army Corps
of Engineers®
Engineer Research and
Development Center

Navigation System Research Program

Experimental Fatigue Evaluation of Underwater Steel Panels Retrofitted with Fiber Reinforced Polymers

Hussam N. Mahmoud, Guillermo Riveros, Lauren Hudak, and
Emad M. Hassan

March 2023

Information Technology Laboratory

DISTRIBUTION A: Approved for public release; distribution is unlimited.

The US Army Engineer Research and Development Center (ERDC) solves the nation's toughest engineering and environmental challenges. ERDC develops innovative solutions in civil and military engineering, geospatial sciences, water resources, and environmental sciences for the Army, the Department of Defense, civilian agencies, and our nation's public good. Find out more at www.erdc.usace.army.mil.

To search for other technical reports published by ERDC, visit the ERDC online library at https://erdclibrary.on.worldcat.org/discovery.

ERDC/ITL TR-23-1
March 2023

Experimental Fatigue Evaluation of Underwater Steel Panels Retrofitted with Fiber Polymers

Guillermo Riveros

US Army Engineer Research and Development Center (ERDC)
Information Technology Laboratory (ITL)
3909 Halls Ferry Road
Vicksburg, MS 39180-6199

Hussam N. Mahmoud, Lauren Hudak, and Emad M. Hassan

Department of Civil and Environmental Engineering
Colorado State University
Engineering Building, Room A203
1372 Campus Delivery
Fort Collins, CO 80523-1372

Final Report

DISTRIBUTION A: Approved for public release; distribution is unlimited.

Prepared for Headquarters, US Army Corps of Engineers
Washington, DC 20314-1000

Under Navigation System Research Program, Work Unit DB5531, Funding Account Code U4376568, AMSCO Code 031391

Abstract

Many steel structures are susceptible to fatigue loading and damage that potentially threaten their integrity. Steel hydraulic structures (SHS) experience fatigue loading during operation and exposure to harsh environmental conditions that can further reduce fatigue life through stress corrosion cracking and corrosion fatigue, for example. Dewatering to complete inspections or repairs to SHS is time consuming and leads to economic losses, and current repair methods, such as rewelding, often cause new cracks to form after relatively few cycles, requiring repeated inspection and repair. The use of bonded carbon fiber–reinforced polymer (CFRP) to repair fatigue cracks in metallic structures has been successful in other industries; recent work suggests that this method offers a more reliable repair method for SHS.

Studies regarding CFRP retrofits of SHS indicate that early bond failure often controls the degree of fatigue life extension provided by the repair. This study aims to extend previous studies and increase the fatigue life of repaired steel components by employing methods to improve CFRP bonding. Additionally, using basalt reinforced polymer (BFRP) instead of CFRP is proposed. BFRP is attractive for SHS because it does not react galvanically and has excellent resistance to chemically active environments.

DISCLAIMER: The contents of this report are not to be used for advertising, publication, or promotional purposes. Citation of trade names does not constitute an official endorsement or approval of the use of such commercial products. All product names and trademarks cited are the property of their respective owners. The findings of this report are not to be construed as an official Department of the Army position unless so designated by other authorized documents.

DESTROY THIS REPORT WHEN NO LONGER NEEDED. DO NOT RETURN IT TO THE ORIGINATOR.

Contents

Figures and Tables

Figures

Tables

Preface

This study was conducted for the US Army Corps of Engineers under the Navigation System Research Program, Work Unit DB5531, Funding Account Code U4376568, AMSCO Code 031391. The technical monitor was Morgan Johnston, Coastal Hydraulics Laboratory.

The work was performed by the Colorado State University Department of Civil and Environmental Engineering, as well as the Computational Science and Engineering Division, US Army Engineer Research and Development Center—Information Technology Laboratory (ERDC-ITL). At the time of publication, Dr. Robert M. Wallace was technical director, and Dr. Jeffrey L. Hensley was division chief. The deputy director of ERDC-ITL was Dr. Jackie S. Pettway, and the director was Dr. David A. Horner.

COL Christian Patterson was commander of ERDC, and Dr. David W. Pittman was the director.

This page intentionally left blank.

1 Introduction

1.1 Background

Many steel hydraulic structures (SHS) in the United States are approaching or have already surpassed their design service lives and are now susceptible to fatigue damage. Fluctuating load patterns are common in numerous civil engineering applications, but for SHS, exposure to underwater environments and therefore accelerated corrosion can contribute to reduced fatigue life in comparison to other steel structures that are operating in less harsh conditions. Due to redundancy in most systems, repairing a single fatigue crack is at times not critical to safety and operation. However, large cracks or widespread cracking in multiple components can threaten the integrity of the structure or at the very least halt a structure's operation. In addition, a structure's remaining fatigue life is difficult to quantify due to scatter in fatigue performance and the possible interaction of multiple flaws (Mahmoud et al. 2018; Mahmoud and Riveros 2014).

Significant and extensive cracking has been repeatedly noted in SHS, especially in locations that are continuously submerged and not easily detectable without dewatering (USACE 2010). Cracks are commonly noted at welded joints, where residual stresses can cause tensile fatigue loading even if the location experiences compressive loading. Figure 1 and Figure 2 show examples of cracked miter gate components that are submerged during operation. Previous repair methods have imitated those used in the bridge industry, such as gouging and rewelding and adding welded cover plates (Mahmoud and Riveros 2013). After repairing and resuming service, these methods do not consistently offer long-term solutions, as cracks tend to reinitiate after relatively few cycles due to newly introduced residual stresses.

Figure 1. Crack near the pintle socket of a miter gate (Mahmoud and Riveros 2013).

Figure 2. Cracks repaired by rewelding in miter gate girder and diaphragm flanges that experience compression loads during gate operation (USACE 2010).

Fatigue cracks in welded joints in the miter gates at the Markland Locks and Dam on the Ohio River, for example, were first observed and repaired by gouging and rewelding in 1984 after 24 years in service. Four years after the first repairs, cracks at the previously repaired locations and new locations were noted. Triangular welded gusset plates were added to reduce stresses at the locations as shown in Figure 2. Six years later, cracking around the gusset plates was noticed, and the gusset plates were replaced with a window frame–type repair as shown in Figure 3, successfully mitigating additional cracking (USACE 2010). While existing repair methods can provide solutions to continue safe operation, frequent

inspection and repair are still required afterwards. This is cumbersome and costly, as dewatering and inspection can require a structure to be temporarily taken out of service.

Figure 3. Welded window frame–type repair implemented for gates at the Markland Locks and Dam.

Due to the challenges with existing repair methods, reliable and simple-to-implement alternatives are of interest. Recent work has proposed that fiber-reinforced polymer (FRP) overlays may offer a solution when used to repair cracks in SHS. FRPs have long been used for general strengthening and repair of structural components, and as summarized by Mahmoud and Riveros (2013), they have been shown to be effective when used to reduce the rate of fatigue crack propagation in metallic structures. However, the applicability of FRP repairs for fatigue in underwater environments has not been fully explored. Exposure to underwater environments accelerates crack growth and can cause damage to and reduce the effectiveness of FRP repairs.

Recent large-scale underwater testing by Mahmoud et al. (2018) demonstrates that carbon fiber–reinforced polymers (CFRP) can be a viable option for underwater repairs, but their effectiveness is limited by poor adhesion to the steel substrate. Figure 4 shows a specimen that was repaired with CFRP and fatigue tested underwater exhibiting substantial CFRP debonding. Some of the debonding can be attributed to corrosion both from the underwater environment and from galvanic interaction between steel and the carbon fibers in contact with each other. When applied over a crack, FRP sheets reduce the stress intensity factor and

therefore the crack propagation rate by reducing the nominal stress on the crack plane and providing a crack closure effect from the fibers that bridge the crack. Both factors rely on bonding between the cracked material and FRP to be effective; therefore, additional work is needed to maximize adhesion in an underwater environment to better increase the fatigue life of repaired cracks.

Figure 4. Carbon fiber–reinforced polymer repair used underwater showing substantial debonding (Mahmoud et al. 2018).

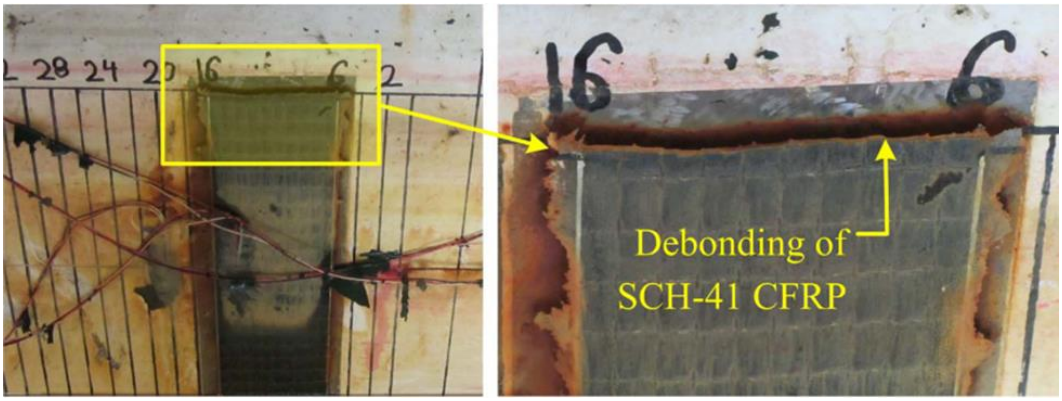

For in-air applications, separation of the carbon and steel by means of an increased thickness adhesive layer or a layer of glass fibers has been used to reduce debonding due to galvanic corrosion. Use of alternative FRP materials other than CFRP, such as basalt fiber–reinforced polymer (BFRP), that do not react with steel can also potentially reduce debonding if the material properties are suitable for the application. Aside from improving adhesion, previous studies on FRP repairs of fatigue cracks have shown improved fatigue life from varying the repair geometry by increasing the width of the FRP sheets to cover more of the crack plane or applying multiple FRP Layers. However, the methods common for enhancing repairs for in-air environments have not been extensively considered for their applicability in underwater environments.

1.2 Objectives and Scope

Before widespread use of FRP repairs for fatigue damage in SHS can be fully realized, a more complete understanding of the effects of an underwater environment is needed. Results from the previously mentioned large-scale experimental work by Mahmoud et al. (2018) indicate that FRP repairs for improving fatigue life underwater are promising but in need of further assessment. Center-cracked steel panels were repaired with CFRP strips adhered ahead of the crack tips on both

faces and fatigue tested to failure. When tested under water, the repair led to a fatigue life improvement of 1.16 times that of an unrepaired specimen underwater. The primary purpose of the work described herein is to build upon and improve the previously tested repair method. By increasing adhesion to steel, the applied FRP is more fully capable of reducing the stress intensity factor experienced by the crack. Varying the FRP repair geometry by increasing the width or using multiple layers can also increase performance.

To accomplish the objective of improving and understanding FRP repairs for SHS, additional experiments needed to be conducted. Center-cracked steel panels similar to those previously tested were fabricated and then repaired. Debonding and corrosion were addressed by using thick adhesive layers, providing a separating layer of glass fiber for specimens repaired with CFRP and introducing the use of BFRP as an alternative to CFRP. Specimens also include variations in repair width and number of FRP layers. Underwater fatigue tests with constant amplitude mode I loading were conducted on each specimen. Results of the tests including fatigue life and crack growth rates can be used to assess the effectiveness of the repair approaches. The following tasks were used to realize the above objectives:

1.2.1 Task 1: Conduct a Literature Review

- Reassess factors most critical to FRP fatigue repairs.
- Evaluate previous use of BFRP for steel structures.
- Identify driving factors of underwater deterioration of steel and FRP.

1.2.2 Task 2: Prepare Test Specimens and Test Setup

- Design test matrix for investigating desired variables.
- Apply the selected retrofit methods to the designated specimens.
- Complete needed maintenance and modifications to the test setup.

1.2.3 Task 3: Execute Experimental Program

- Submerge specimens in water tank
- Apply fatigue loading to induce crack growth
- Collect readings of strain in steel and FRP
- Record crack length with corresponding number of cycles
- Observe bond behavior of FRP

1.2.4 Task 4: Interpret Experimental Results

- Evaluate and compare crack growth results across specimens
- Interpret recorded strain in FRP in conjunction with visually observed behavior
- Identify failure modes
- Assess effectiveness of CFRP and BFRP repairs

1.3 Approach

This study comprises five sections. Section 1 addresses the need for an improved repair method for SHS with existing cracks and describes the purpose of this research toward meeting that need. Section 2 includes a literature review and background information regarding repair of structures with FRPs and their applicability to underwater environments. The experimental approach and test setup are provided in Section 3. This includes details of the configuration of each specimen and the purpose of the selected configurations. Results and discussion of the completed tests are presented in Section 4. Section 5 concludes the study by summarizing the findings of the work and identifying additional matters to be addressed in future work.

2 Background and Literature Review

2.1 Introduction

Use of CFRP for repair of metal alloys has been well explored in recent years, although field use is still limited. Various experimental studies, several field applications, and multiple numerical and analytical modeling approaches have been thoroughly reviewed by Mahmoud and Riveros (2013) to assess the applicability of CFRP use for SHS. Additionally, Riveros et al. (2019) covered the underlying fatigue and fracture topics related to fatigue crack repairs. Topics most critical to the success of CFRP fatigue crack repairs are reiterated in this section. Additionally, the factors introduced for underwater repairs and the proposed use of BFRP as an alternate to CFRP are considered.

2.2 Overview of Carbon Fiber–Reinforced Polymer Repairs of Center-Cracked Panels

Several examples of experimental programs using CFRP bonded to steel as a fatigue crack repair method are available, and many express a purpose of repairing steel bridge components. Mahmoud and Riveros (2013) conducted a review of related experimental work, on metal alloys in general and steel structures specifically, as part of a feasibility study for CFRP repairs to hydraulic structures; this study can be referenced for a thorough assessment of previous experimental research. Here, the studies and topics most pertinent to the current experimental work are covered to highlight factors that affect the performance of CFRP when used to repair center-crack tension fatigue specimens.

2.2.1 Factors Contributing to Carbon Fiber–Reinforced Polymer Fatigue Repairs of Center-Cracked Panels

Two primary mechanisms from the addition of CFRP patches contribute to reducing fatigue crack growth (Colombi 2004). First, increased stiffness from the patches reduces the nominal stress felt by the crack. Second, CFRP that bridges an existing crack limits the crack opening displacement. From the first mechanism, it follows that any increase in the stiffness of CFRP in the cracked cross section can improve performance. The second mechanism only contributes if the CFRP is covering the crack. Increased stiffness also promotes reduction in crack opening displacement, but it is additionally imperative for the CFRP to be covering or as near as possible

to the existing crack to utilize the reduced crack opening effect. If the existing crack is not covered, the second mechanism is utilized only once the crack has propagated far enough to interact with the CFRP (i.e., the crack extends under the CFRP patch). When extended, the fibers bridging the crack apply a compressive force that promotes crack closure. The effect is similar to that of compressive residual stresses that exist between stiffeners and reduce the crack rate in welded stiffened panels as demonstrated in several studies (Dexter et al. 2005, 2003; Mahmoud and Dexter 2005).

The method of increasing cross section stiffness by using high modulus CFRP was demonstrated by Liu et al. (2009*a*) and Colombi and Fava (2015). High modulus CFRP is significantly more effective at improving fatigue life than an identical application of lower modulus CFRP. However, because higher modulus CFRP requires a greater stress to be transferred through the adhesive layer, adhesive can be more prone to debonding from steel during fatigue loading compared to when lower modulus CFRP is used if care is not taken to select an appropriate adhesive (Jones and Civjan 2003).

Using thicker CFRP patches to increase the cross section stiffness also improves fatigue life in comparison to using a thinner layer as demonstrated by Liu et al. (2009*a*) and Colombi and Fava (2015). However, when a larger thickness is achieved by applying multiple layers of CFRP, the effectiveness of each subsequent layer is less than the previous layers due to reduced stress transfer to the outer layers (H. Liu et al. 2009*b*; Riveros et al. 2018). Therefore, there may be a point when additional layers no longer provide significant benefit in terms of stress reduction at the crack tip.

Varying the width of applied CFRP patches can change the cross section stiffness and, in conjunction with patch location along the crack plane, change the length of existing crack that is covered and experiencing reduced crack opening displacement. The CFRP configurations used by G. Wu et al. (2012) demonstrate the use of varying widths and locations along the crack plane. Each CFRP configuration was applied to both sides of a steel plate with a crack initiator at the center, and specimens were fatigue tested with maximum stress of 150 megapascals (MPa) and stress ratio of 0.1 in the horizontal direction, as shown in Figure 5. With maximum width and CFRP covering the initial crack, configuration (a) entirely arrested the

crack. The other configurations still significantly increased fatigue life when compared to a specimen with no repair with an order from most to least improvement of (b), (e), (c), and (d), as shown in Figure 6. Results indicate that there is less improvement when the crack is not covered and, if not covered, when the patch is farthest away from the initial crack. Additional results found by Jones and Civjan (2003) with similar style tests showed fatigue life was improved by 170% when the initial crack was covered and 115% when it was not.

Figure 5. Repair configurations used by G. Wu et al. (2012) (hatched areas represent carbon fiber–reinforced polymer, dimensions in millimeters).

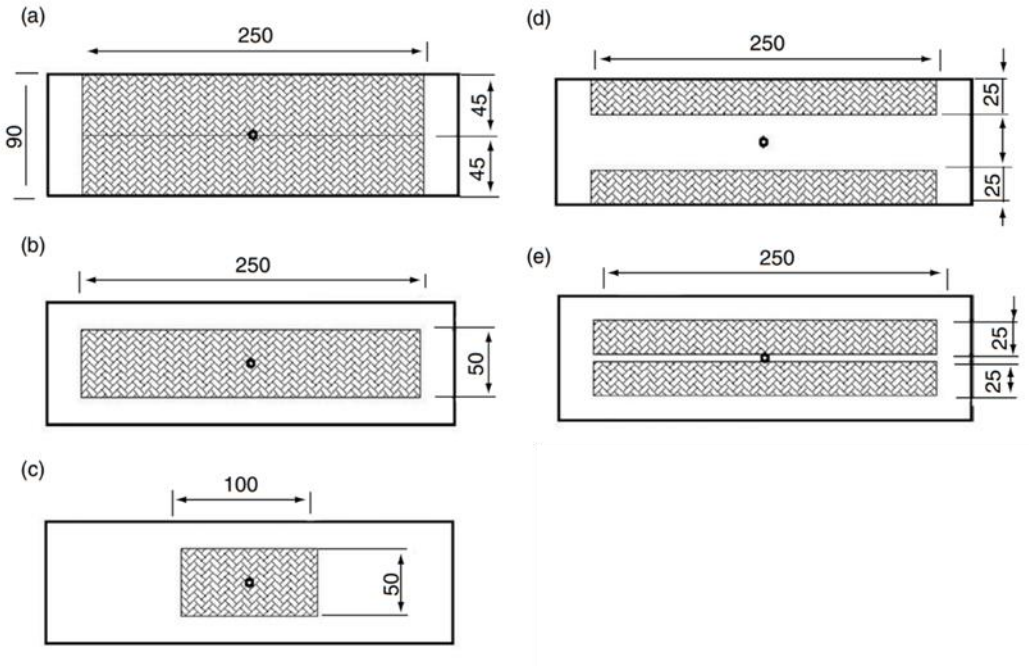

Figure 6. Crack growth results for various configurations as tested by G. Wu et al. (2012).

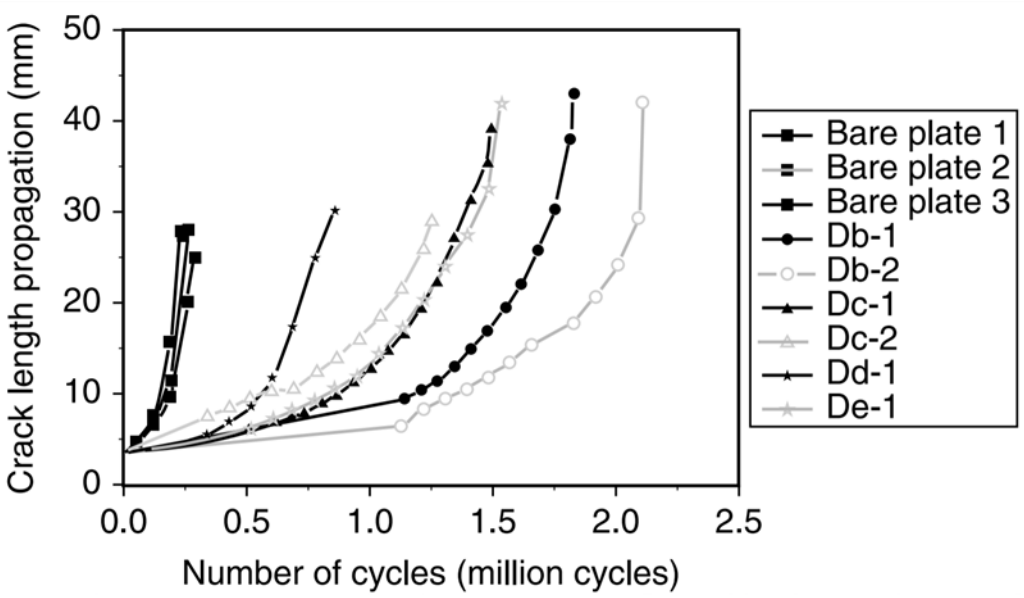

When comparing configurations (b) and (c) from G. Wu et al. (2012), it is clear that the length of an applied CFRP patch also contributes to repair effectiveness. However, performance is reduced only when the CFRP length is less than the effective bond length. The effective bond length is the smallest length at which a maximum possible stress is reached in the CFRP (Nozaka et al. 2005). Using a length greater than the effective length provides little to no additional benefit. Effective bond lengths for CFRP with steel substrate have been experimentally determined and estimated with empirical, analytical, and numerical models by both H. Liu et al. (2007) and Nozaka et al. (2005).

Several studies have compared the use of single- and double-sided application of CFRP for fatigue repairs of cracked plates in tension (Jones and Civjan 2003; H. Liu et al. 2009*a*; Mahmoud et al. 2014; Zheng et al. 2006). While single-sided repairs have shown to be effective, double-sided repairs perform much better because a single-sided repair of a tensile member causes an eccentric load path, leading to added bending stresses in the steel.

2.2.2 Methods for Improving Fiber-Reinforced Polymer Bonding

Although use of bonded CFRP to repair fatigue cracks in steel has been shown to be effective, debonding between adhesive and steel is common in previous testing and can significantly limit the repair effectiveness

(Bocciarelli et al. 2009; Colombi et al. 2003; Colombi and Fava 2015; Jones and Civjan 2003; Monfared et al. 2008; Riveros et al. 2019; Tavakkolizadeh and Saadatmanesh 2003; Zheng et al. 2006). Debonding generally occurs where a stress concentration exists in the adhesive layer. Predominantly, debonding begins either at the end of the CFRP patch or adjacent to the fatigue crack. The debonded portion then propagates beneath the CFRP, progressively reducing its effectiveness.

It may be possible to avoid any debonding at the CFRP patch ends as evidenced by fatigue crack repair studies that did not observe any debonding prior to the final failure (H. Liu et al. 2009*a*; Mertz and Gillespie 2002; C. Wu et al. 2013; Zhao and Zhang 2007), and studies focused primarily on fatigue of CFRP bond to steel report no debonding below threshold stress levels (Deng and Lee 2007; H. Liu et al. 2005; Matta et al. 2005). The composite and adhesive properties selected must be appropriate for the required loading, and the loading must be relatively low. H. Liu et al. (2005), for example, found that bonds in double strap joints between steel and CFRP did not experience fatigue failure if the maximum fatigue stress was less than approximately 40% of the joint's ultimate strength.

Debonding adjacent to the fatigue crack likely cannot be prevented due to the very high strains near the crack tip, but reduced debonding at the crack may be attainable. Colombi et al. (2003) report that delamination around the crack occurs in an elliptical shape with a width that spans between the plastic zones at either end of a crack and a height that can vary depending on the system properties. Analytical models, such as that used by Lozano and Riveros (2019), can be used to determine the local debonding near the crack. Lozano and Riveros (2019) used results from Mahmoud et al. (2018) for validation and found good agreement.

Bond between CFRP and steel can be improved by increasing the adhesive layer thickness because a larger shear deformation can be achieved before debonding occurs (Colombi et al. 2003). Using an adhesive with high ductility similarly allows for more deformation before debonding (Nozaka et al. 2005). However, increasing the adhesive deformation can reduce the repair effectiveness because stress is less efficiently transferred from the steel to the CFRP. In locations where a patch covers the crack, adhesive deformation allows for a larger crack opening displacement (Colombi et

al., 2003). Despite reduced effectiveness due to thicker adhesive, preventing sizable debonded regions is more critical.

If material properties of the system cannot be modified to provide better bonding, several other techniques can be used to prevent debonding at patch ends. The use of a spew fillet around the edges of CFRP patches, as shown in Figure 7, is known to reduce the stress concentration at the end of the adhesive as suggested by Bocciarelli et al. (2009), Deng and Lee (2007), and Shield et al. (2004). Mechanical clamps, such as the example shown in Figure 8, can also be used to apply pressure at the end of CFRP patches to prevent debonding (Gangel 2011; Vatandoost 2010).

Figure 7. Sketch of cross section with adhesive spew fillet (Shield et al. 2004).

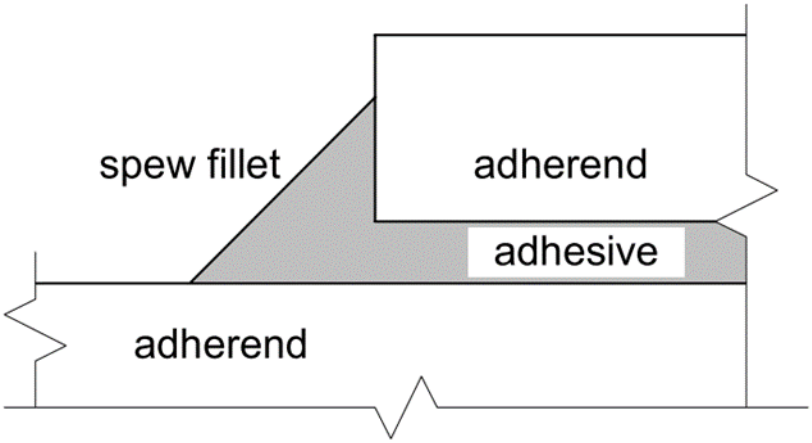

Figure 8. Clamp made from steel plates and pretensioned bolts to prevent carbon fiber–reinforced polymer debonding (Gangel 2011).

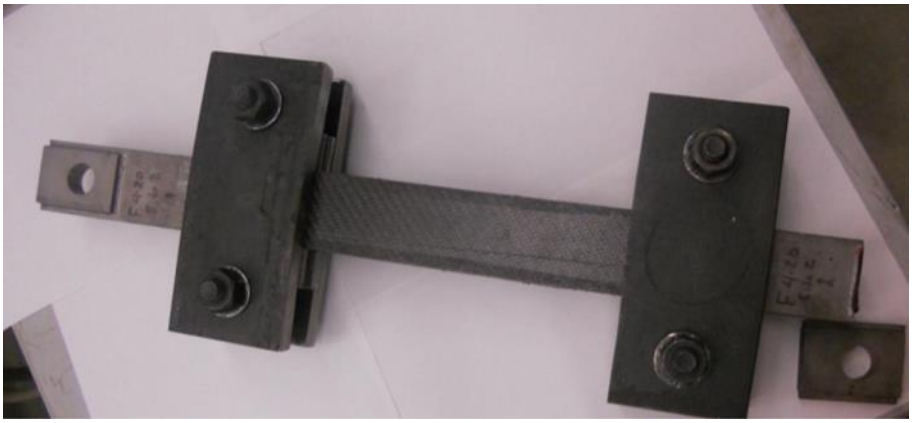

An additional consideration for the bond between CFRP and steel is galvanic corrosion. When two dissimilar metals are in direct contact, a galvanic cell is formed, and the anode, which is steel in the case of steel

and CFRP contact, corrodes (Tavakkolizadeh and Saadatmanesh 2001). Corrosion forming between the CFRP and steel deteriorates the bond. To prevent galvanic action, the carbon and steel must be insulated from each other. A thick layer of adhesive has been shown to be effective at reducing galvanic action (Tavakkolizadeh and Saadatmanesh 2001). It is also common to use a layer of glass fiber fabric between steel and CFRP as insulation (Hollaway and Cadei 2002; H. Liu et al. 2009*b*; Mertz and Gillespie 2002; Zhao and Zhang 2007).

2.3 Use of Basalt Fiber–Reinforced Polymer

Use of BFRP in civil engineering applications is new and limited to only a few studies. A basalt and steel wire hybrid composite was used by G. Wu et al. (2012) to repair steel beams in fatigue, and BFRP was used by Jayasuriya et al. (2018) to restore the strength of steel beams with corrosion damage, but no other instances of BFRP used with steel structural components are known.

A key benefit of BFRP for applications to steel is that it does not cause galvanic corrosion. Basalt is not a conductor (Jayasuriya et al. 2018), so there is no concern of dissimilar metals coming in contact, as previously discussed with regard to carbon. Use of basalt may improve bonding in comparison by eliminating galvanic corrosion completely. Additionally, BFRP installation can be simplified because an extra step to insulate the FRP from the steel substrate is not necessary.

Mechanical properties of basalt fiber can vary widely, but basalt fibers have lower tensile strength and modulus than carbon fibers and higher tensile strength and modulus than glass fibers (G Wu. et al. 2012; Z. Wu 2010). Since strength is generally controlled by the bond rather than the fibers for the proposed type of fatigue crack repairs, the reduced strength of BFRP compared to CFRP is not of highest concern. FRP stiffness, however, contributes significantly to repair effectiveness, and the lower modulus of BFRP would tend to reduce the crack closure effect.

It may be possible to account for the lower modulus of BFRP by using a larger thickness of BFRP when comparing its use to CFRP to obtain equivalent stiffnesses, as was done by G. Wu et al. (2012). A variety of FRP types were used to repair notched steel beams tested in fatigue with thicknesses adjusted for each type to maintain the same stiffness of the repair across specimens. Comparable results for fatigue life improvement

were found for the composites tested despite their variations in tensile modulus.

Due to previous use in other industries, fatigue life of BFRP has been studied. BFRP does not perform as well in fatigue as CFRP. Dorigato and Pegoretti (2012) developed S-N (alternating stress versus number of cycles to failure) curves for carbon, basalt, and glass fiber laminates in tensile fatigue, as shown in Figure 9. The slope of the S-N curve for BFRP is dramatically steeper than that for CFRP, indicating a reduced fatigue life in comparison to CFRP. Fatigue limits for CFRP and BFRP determined by Z. Wu et al. (2010) indicated that BFRP has infinite life under constant amplitude fatigue when the stress is less than 55% of its tensile strength, whereas the same is true for CFRP when the stress is less than 84% of its tensile strength. Due to the lower fatigue resistance of BFRP, more fatigue life consideration of the composite may be needed when BFRP is used as an alternative to CFRP in fatigue repairs.

Figure 9. S-N curves for glass, basalt, and carbon FRP developed by Dorigato and Pegoretti (2012).

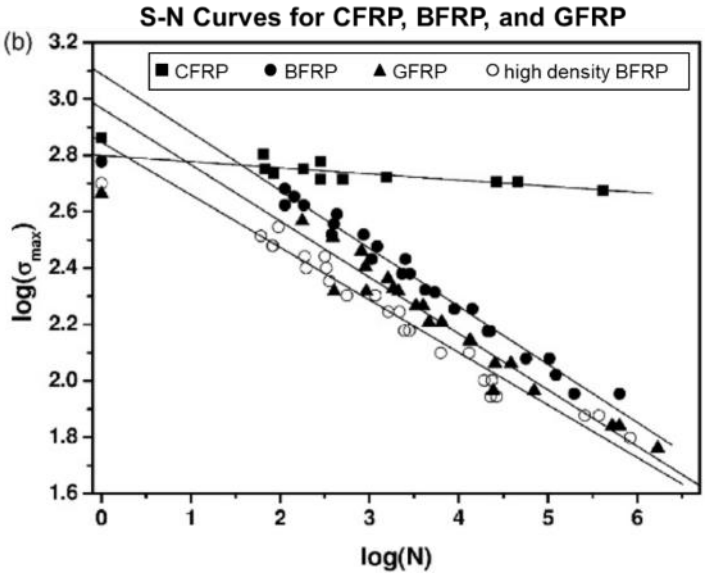

2.4 Underwater Fiber-Reinforced Polymer Repair of Fatigue Cracks

The fatigue life of unprotected steel is reduced in an underwater environment, and the deleterious effect is known as corrosion fatigue. In addition to increased crack growth in steel due to the underwater environment, FRP repair methods may also be less effective when exposed to water. Although these effects are recognized, they are difficult to assess

due to time dependence. In comparison to underwater structural repairs that can often be in place for many years, the time spans of existing experimental studies are short. It is possible that degradation may continue to increase with longer exposure time; however, information is limited because use of composites in civil engineering and especially in underwater environments is relatively new.

2.4.1 Underwater Fatigue Crack Growth in Steel

In comparison to fatigue in air, corrosion fatigue is more complex and requires the consideration of more variables such as load frequency and chemical properties of the water. Although the exact contributions to corrosion fatigue remain unclear due to difficulty in differentiating between all mechanisms during experimentation, hydrogen embrittlement and anodic dissolution are commonly identified as the main driving factors (Gangloff 2009; Kang et al. 2011; Salivar et al. 1981). Hydrogen embrittlement increases crack growth rate by making the material around the crack more brittle. Hydrogen in water absorbs into crack surfaces and interferes with grain boundary cohesion. Anodic dissolution occurs as the newly exposed material from crack growth reacts with the water and is dissolved (Gangloff 2009).

In air, loading frequency has little effect on fatigue crack growth rate in steels. However, in underwater environments, frequency becomes an important factor due to the time dependence of the chemical reactions that contribute to increased growth rates. A testing regime using lower frequency allows more time for reaction and therefore results in a more pronounced increase in crack growth underwater compared to in air. An experimental study conducted by Salivar et al. (1981) considered crack propagation in steel in air, distilled water, and saltwater environments with varying frequencies. Wedge opening load type specimens with 1-inch thicknesses were tested in air and in a chamber containing either distilled water or a 3.5% NaCl solution. A frequency of 10 Hz in air was used as a baseline for comparison with other scenarios. For both distilled water and salt water, frequencies of 10 Hz, 1 Hz, and 0.1 Hz were tested. Resulting crack growth rates showed no significant difference between the three environments for the highest frequency of 10 Hz. For the lower frequencies, the underwater environments caused significantly higher crack growth rates, with crack growth rate increasing with decreasing frequency. However, there was no significant difference between results for the distilled water and saltwater environments. Hydrogen

embrittlement was attributed to the increased crack rates underwater as a result of the fractography analysis of the crack surfaces that was conducted and showed intergranular fracture was present when the growth rate was increased in underwater environments.

Similarly, varying the stress range can indirectly introduce a time variable that affects fatigue life underwater. If maintaining all other variables, reducing the stress range lowers the crack growth rate and therefore increases the time required for a crack to grow to a given length. If underwater, the increased time needed for crack growth allows the environmental factors a longer time to react, resulting in more pronounced degradation. This can result in a larger difference between fatigue life in air and water with lower stress ranges compared to higher stress ranges. Plots of stress range versus number of cycles for air, fresh water, and saltwater environments were developed and compared by Morgantini et al. (2018). Round rod specimens were axially fatigue tested with varying stress ranges and stress ratios in the three environments. Comparing the resulting S-N curves for fresh water and air, as shown in Figure 10, indicates that the environmental factors are much more present with low stress ranges. At higher stress ranges, at which the tests took fewer than 106 cycles, the results in water showed little difference from those in air. However, at the lowest stress ranges tested, which approached 107 cycles, the fatigue life was reduced by a factor of 2.1 when in water. The authors attribute this to the larger amount of time in water when the stress range is low. Also, the fatigue limit for the underwater environment was not reached in the stress ranges that were tested, which implies that the life reduction could be even greater with lower stress range. Comparing the resulting S-N curves in fresh water and salt water as shown in Figure 11 shows that salt water reduces fatigue life more than does fresh water, but the difference is very small compared to that between fresh water and air.

Figure 10. S-N curves for steel in air and fresh water corrosion fatigue (CF) (Morgantini et al. 2018).

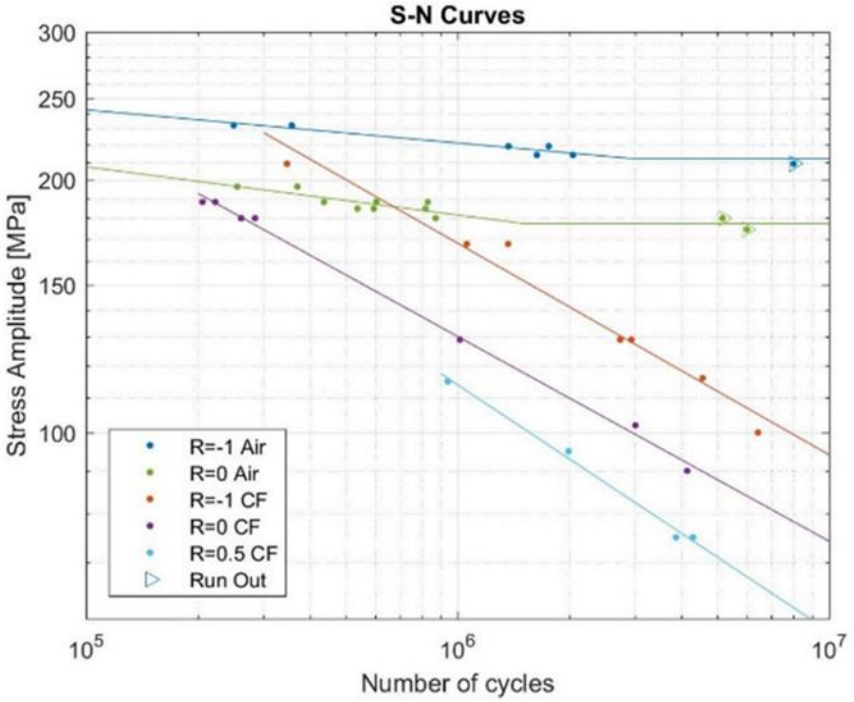

Figure 11. Comparison of S-N curves for steel in fresh water and salt water (Morgantini et al. 2018).

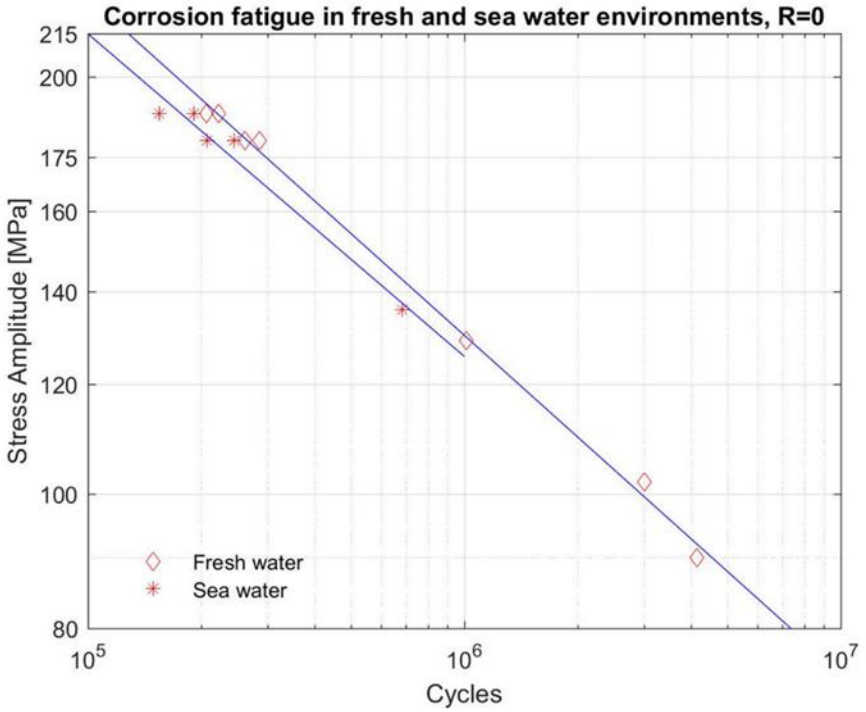

As one of the driving factors of corrosion fatigue is hydrogen embrittlement, which is caused by a reaction between steel and hydrogen,

it is logical that the pH of the environment may affect fatigue life. Differences in fatigue life between steel in solutions of various acidities were explored by Misawa and Kobayashi (1976). Round rod specimens with 15 mm diameter and 2.5 mm machined notches were tested in a rotating-bending fatigue machine. A corrosion cell around the specimens contained water with pH of 0.5, 5.3, or 11.2. Crack length and number of cycles were recorded throughout each of the tests. The solution closest to neutral, with a pH of 5.3, resulted in the highest fatigue life. Both the acidic and basic solutions reduced the life; however, it was reduced significantly more with the acidic solution, as depicted in Figure 12. This suggests a complex relationship between the pH of water and fatigue life of steel.

Figure 12. Fatigue crack propagation of steel in solutions of varying pH (Misawa and Kobayashi 1976).

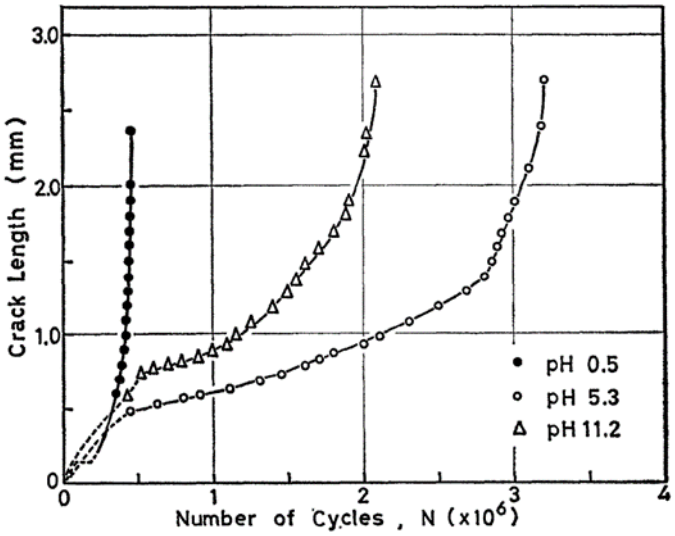

2.4.2 Underwater Bonded Fiber-Reinforced Polymer Durability

As with in-air repairs, underwater repairs with FRP have been explored more for concrete than steel applications. Several examples of applying FRP to deteriorated concrete in tidal zones have been completed (Al Azzawi et al. 2018; Long et al. 2012). Mahmoud and Riveros (2013) provided a small number of examples of CFRP used for repair of ship structures. However, no examples of FRP used underwater for fatigue repair in steel other than those by Mahmoud et al. (2018) and Riveros et al. (2018) are known. Although limited previous work has shown that tensile strength, elastic modulus, fatigue life, and bond of FRP can be reduced when underwater.

Changes in tensile strength and elastic modulus of various FRP—including CFRP and BFRP—after exposure to aqueous solutions were studied by Liu et al. (2017). Coupons were subjected to wet-dry cycles where they were submerged for 15 days and then in air for 15 days. Tensile tests to obtain ultimate strength and tensile modulus were conducted after between 1 and 12 wet-dry cycles were completed. Sulfate, chloride, alkaline, and acidic solutions were used. The CFRP samples were minimally affected by all of the solutions, with maximum reductions after 12 cycles of 10% and 5% for tensile strength and modulus, respectively. However, BFRP was more significantly degraded after 12 cycles with tensile strength reductions between 13% and 34% depending on solution type and tensile modulus reductions of approximately 15%.

In air, CFRP is well known for its high fatigue strength. CFRP coupons exposed to moisture were tested in bending fatigue and compared to dry specimens by Meng et al. (2016). Samples were submerged in fresh water or sea water for three months prior to testing, and moisture was maintained during testing by wrapping them with saturated sponges. Tests used constant amplitude four-point bending with a stress ration of 0.1 and various maximum stresses. Although resulting fatigue lives were scattered, saturated specimens clearly showed reduced life in comparison to dry specimens. Dry specimens tended to have infinite life, which was taken as no sign of failure after 106 cycles, if the maximum stress was less than 80% of ultimate strength. For saturated specimens, the life was generally only infinite if the maximum stress was less than 65% of ultimate strength.

The adhesives used for FRP can also be susceptible to damage from exposure to water. Water can diffuse into adhesives and chemically react (Hollaway and Cadei 2002). It is possible for the adhesive to plasticize or breakdown and crack. Adhesive deterioration due to moisture exposure is known to be time dependent. However, no example of environmental testing with extended durations that would be applicable for civil engineering structures with long services lives is known, and accelerated testing methods do not represent the environments experienced in service well (Hollaway and Cadei 2002).

3 Experimental Program

3.1 Introduction

The experimental program consisted of testing eight center-cracked steel panels, six of which were retrofitted with different configurations of FRP, subjected to constant amplitude mode I fatigue loading. Both BFRP and CFRP were used to evaluate BFRP as an alternative to CFRP. Specimens were submerged in fresh water to simulate the service environment experienced by SHS. The specimen design, test frame, and procedure are similar to those previously used by Mahmoud et al. (2018).

3.2 Text Matrix and Specimen Details

A total of eight center-cracked Tension (CCT) panels were tested with dimensions of 1 m × 1 m (3.28 ft × 3.28 ft), a thickness of 9.5 mm (3/8 in.), and centered 102 mm (4 in.) precut crack as shown in Figure 13*a*. Additionally, because only crack propagation, not initiation, was of interest, tack welds were placed at the ends of the pre-cut crack to promote the initial step of crack propagation from the precut crack. One unretrofitted specimen (specimen S1) was tested in the air (dry condition) to establish a baseline and determine the reduction in fatigue life caused by the underwater environment. Another unretrofitted specimen (specimen S2) was tested in freshwater to establish a baseline comparison against the repaired specimens. No retrofitted specimens were tested in air conditions, which was previously covered by Mahmoud et al. (2018) to investigate the effectiveness of FRP repair in dry conditions.

Four specimens were retrofitted with two double layers of FRP patches on each face. The retrofitted specimens were tested in freshwater to simulate the environment experienced by SHS. Treated freshwater was used as a baseline condition as opposed to untreated river water. An FRP patch width of 178 mm (7 in.) was selected based on the manufactured width of the fiber fabric that was used. A patch length of 381 mm (15 in.) was used. All repaired specimens used two layers of FRP on each face. CFRP and BFRP patches were used for specimens S3 and S5 and specimens S4 and S6, respectively. To ensure repeatability of the results, the specimens repaired with two FRP patches are repeated (i.e., specimen S5 is identical to specimen S3 and specimen S6 is identical to specimen S4). The retrofit

method and test environment for each specimen are summarized in Table 1. Figure 13*b* shows the dimension of the retrofitted specimens.

Figure 13. Specimen configuration: (*a*) air specimen, (*b*) two patches specimen, (*c*) full patch specimen, and (*d*) cross-sectional view of the fiber-reinforced polymer patches.

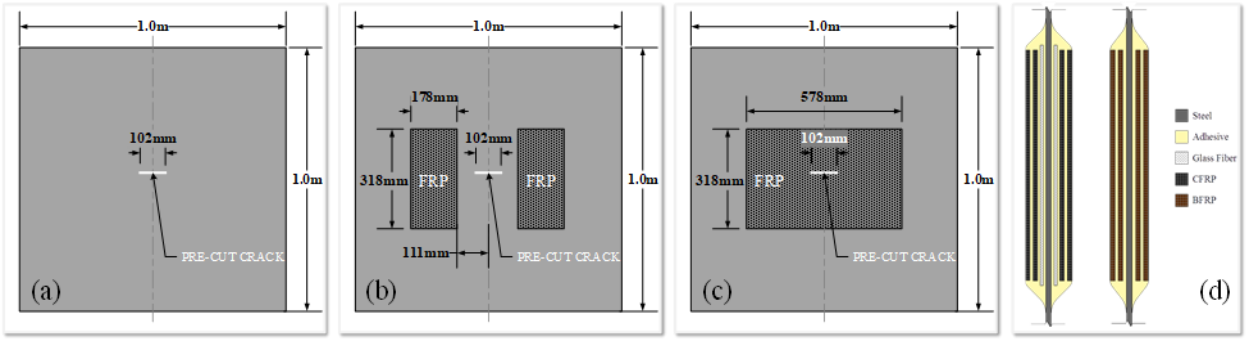

Table 1. Test matrix.

Specimen	FRP Type	FRP Layers	FRP Configuration	Environment
S1	None	0	None	Air
S2	None	0	None	Fresh water
S3	Carbon	2	Two patches	Fresh water
S4	Basalt	2	Two patches	Fresh water
S5	Carbon	2	Two patches	Fresh water
S6	Basalt	2	Two patches	Fresh water
S7	Carbon	2	Full patch	Fresh water
S8	Basalt	2	Full patch	Fresh water

To investigate the effect of applying a more aggressive repair, two specimens were repaired with two layers of full patches on each face. The repairs completely covered the pre-introduced cracks to limit crack tip opening displacement. Specimen S7 was repaired with CFRP, while specimen S8 was retrofitted with BFRP. The two retrofitted specimens were also tested in freshwater and under the same environment as the previous retrofitted specimens. An FRP patch with width of 578 mm (22 3/4 in.) and length of 381 mm (15 in.) was used. The retrofit method and test environment for each specimen are summarized in Table 1. Figure 13*c* displays the dimension of the retrofitted specimens.

An adhesive epoxy was used between the steel and FRP patch and between subsequent layers of FRP to improve bonding. A spew fillet was also

formed from the adhesive around the perimeter of the FRP patch to reduce stress concentrations and reduce the potential for debonding at the patch ends. For the specimen repaired with CFRP, an additional layer of glass fiber fabric was installed between the steel and CFRP to provide an insulating barrier and prevent galvanic corrosion. Cross-sectional views of the FRP patch locations are illustrated in Figure 13*d*.

3.3 Material Properties

Both types of FRP were made from unidirectional fiber fabrics that were saturated with epoxy to form composites. The carbon fabric used was Tyfo SCH-41, manufactured by Fyfe Co. The basalt fibers used were manufactured by Textum. Tyfo S epoxy made by Fyfe Co. was used as the saturant epoxy for both fiber types. Tyfo TC epoxy made by Fyfe Co. was used as the adhesive. The mechanical properties of materials are provided in Table 2. Since the basalt fiber properties are unknown, ranges are listed in Table 2 as found in the literature (Dorigato and Pegoretti 2012; F. T. Liu et al. 2017; G. Wu et al. 2012; Z. Wu et al. 2010). The plates used were structural rolled steel with 9.5 mm (3/8 in.) thickness. A bi-directional glass fiber fabric was used for the insulation for the CFRP repaired specimen.

Table 2. Material properties.

Material	Tensile Strength (MPa)	Tensile Modulus (GPa)
Steel	250	200
Carbon fiber (Tyfo SCH-41)	4,000	230
Basalt fiber	1,200–2,200	65–90
Saturant epoxy (Tyfo S)	72.4	3.18
Adhesive epoxy (Tyfo TC)	22.7	1.2

Average thickness of the CFRP measured from coupons was approximately 2 mm. For the BFRP, average measured thickness from coupons was 3 mm. The CFRP and BFRP were not intended to have equivalent stiffness, though the larger thickness of the BFRP can partially account for its reduced tensile modulus in comparison to the CFRP. Although adhesive application was not perfectly even, the average thickness of an adhesive layer was approximately 3 mm.

3.4 Specimen Manufacture and Retrofit Application

Each specimen was cut to size from 9.5 mm (3/8 in.) rolled steel plates, and then holes for connection to the testing frame were made with a magnetic drill. The existing crack was first cut with a 102 mm (4 in.) diameter and 3 mm (1/8 in.)-thick angle grinder disk and then cut to square with a reciprocating saw. Tack welds, approximately 6 mm (1/4 in.) in diameter, were added at the ends of the cracks to promote crack initiation.

For the retrofitted specimens, outlines of the FRP patch locations were marked, and an angle grinder was used to clean and roughen the surface within the patch locations. The roughened surfaces were then thoroughly cleaned with acetone to remove particles from grinding, and the patch locations were re-marked. The required carbon, glass, and basalt fiber fabrics were cut to size and wiped with a cloth dampened with acetone to remove any dust. Glass fibers were cut approximately 13 mm (1/2 in.) larger in both dimensions than the carbon fibers to ensure an adequate insulating layer should there be any slight misalignment during application.

The FRP patches were applied with a wet layup process. Proper adhesion and fiber alignment were critical during the application process because they are important for the performance of the retrofit. However, the installation process was not intended to be highly precise because it is ultimately intended to be feasible for applications in the field, not just a controlled laboratory environment.

The adhesive (Tyfo-TC) and saturant (Tyfo-S) used are both two-component epoxies, and they were mixed according to manufacturer instructions. Each component was measured by weight, and an electric mixer was used to blend for the specified amount of time. The time was noted after mixing each batch of epoxy, and new batches were made as needed based on the manufacturer-specified pot life.

FRP patches were applied one at a time. Adhesive was spread on the clean, roughened steel surface in a uniform layer using a spatula. A layer of fibers was then placed on top of the adhesive and gently pressed into the adhesive and smoothed to remove any air bubbles and align fibers. Additional alternating layers of adhesive and fibers were applied as needed for each specimen. Before being placed, carbon fibers and basalt fibers

were saturated with Tyfo-S. Fibers were fully submerged in the saturant and then removed and gently stripped of excess by hand. Placement was such that the unidirectional fibers were aligned perpendicular to the crack plane. The glass fiber fabric layers were not saturated.

After all the layers were applied, spew fillets around the patches were formed by hand from additional adhesive to create a smooth transition between the patch and the steel. Any spilled or excess epoxy on the specimen was then removed. The epoxies were allowed to harden before being handled, and the manufacturer-specified cure time was observed. All retrofits were performed in normal temperature and dry conditions, which represents reality since miter gates are typically dewatered prior to the implementation of any major repairs. The FRP application process is illustrated in Figure 14.

Figure 14. Fiber-reinforced polymer patch retrofit application process.

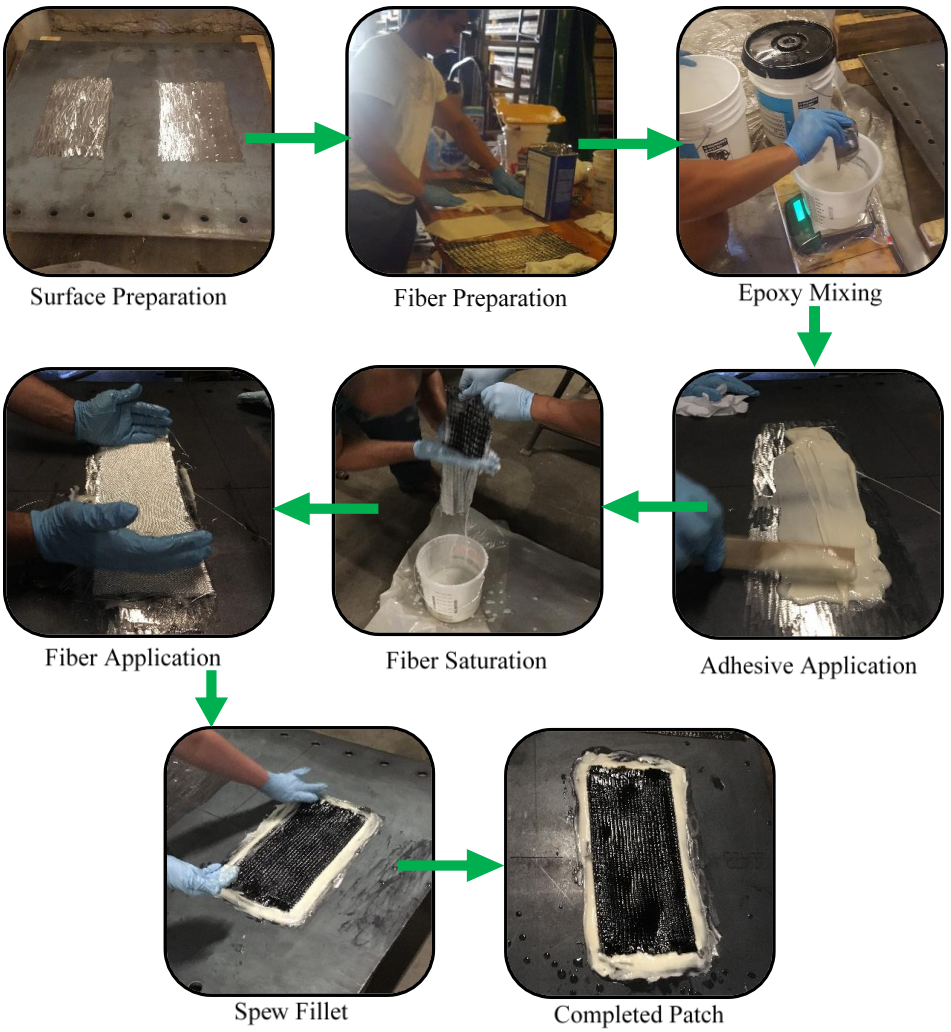

3.5 Test Setup

A self-reacting steel frame was designed to support the specimen and MTS hydraulic actuator and resist the cyclic load applied to the specimen. Conceptually, the test frame was identical to that used by Mahmoud et al. (2018), but beam and column sizes were increased to extend the frame's fatigue life. Once installed, specimens were positioned such that the faces of the steel plates were oriented to the north and south and cracks would propagate to the east and west. Specimens were attached to the lower beam using a double angle connection. Another double angle connection at the top of the specimens attached a stiffened built-up I-beam used to distribute load from the actuator. The actuator was secured to the test frame's upper beam with threaded rods that spanned from the actuator

through to the top flange of the beam. Strain gauges on the rods were used to monitor pretensioning of the rods. All bolts in the test frame were pretensioned using direct tension indicating washers.

A tank surrounding the specimens was built for use when an underwater test environment was needed. The steel tank floor rested on the lower test frame beam. Acrylic sheets were used as tank walls so that the specimens could be observed from outside the tank. Pumps were installed so that the tank could be easily filled and drained when needed. A schematic of the test frame and water tank as viewed looking south is provided in Figure 15. A photo of the test system viewed looking south is shown in Figure 16.

Figure 15. Schematic of self-reacting test frame looking south.

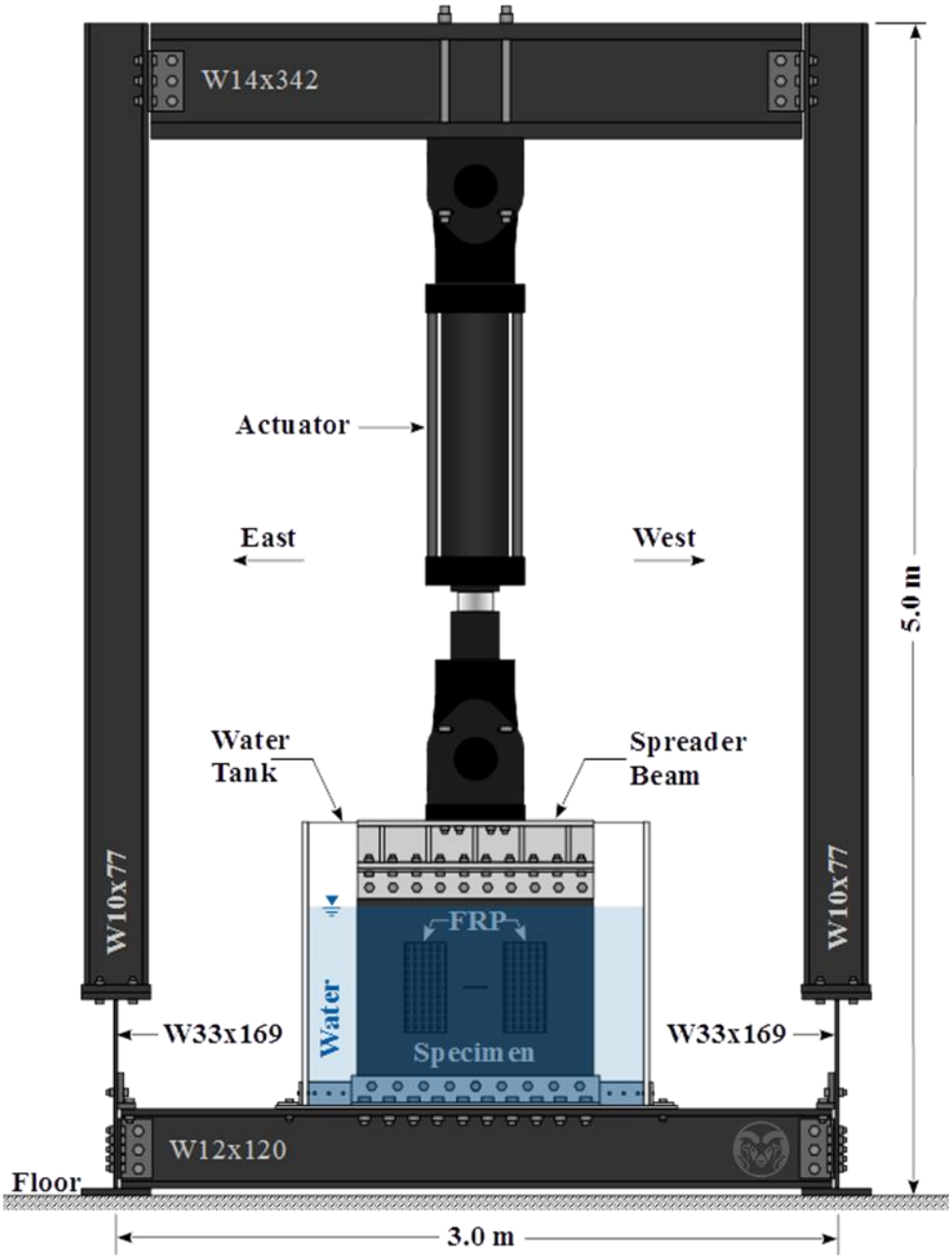

Figure 16. Photo of test frame.

3.6 Instrumentation

Strain gauges were installed on each specimen as shown in Figure 17. Strain gauges located above the crack plane were used to verify the applied nominal stress. All specimens had multiple strain gauges installed along the crack plane. Unlike the strain gauges attached to the steel panel, the gauges located on the patches are attached directly on the FRP sheets to monitor their strain. Strain values from these gauges were expected to increase with crack growth and grow rapidly as the crack approached a gauge. For the retrofitted specimens with two patches, additional strain gauges were used to monitor FRP debonding, if any, by placing them along

the height of the patches. For the retrofitted specimens with a full patch, additional strain gauges on the FRP and above the crack were utilized to monitor the crack's initial growth. A drop in a reading from a gauge on the FRP indicated that the bond directly beneath it was no longer intact. Strain gauges applied to specimens S2 through S8 were covered in silicone sealant to protect them from the water. A National Instruments PXI data acquisition system was used for recording strain readings.

Figure 17. Specimen 1 strain gauge layout.

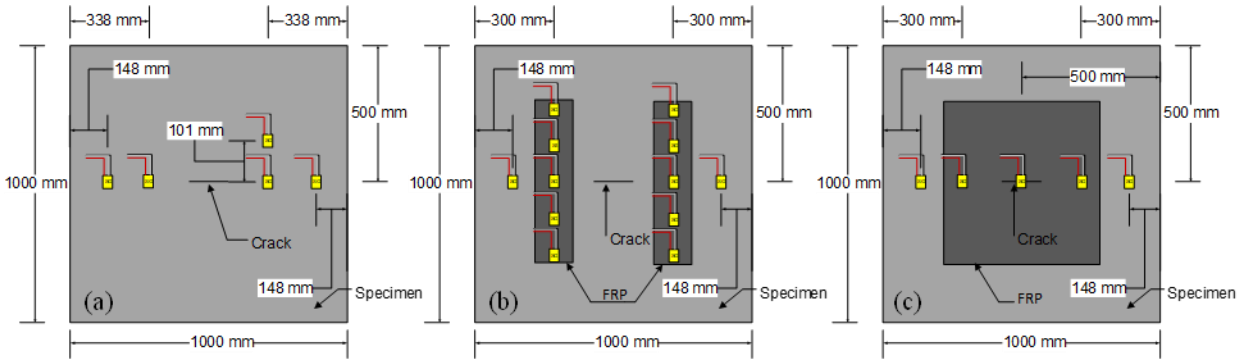

3.7 Test Procedure

Specimens were subjected to a constant amplitude fatigue load with amplitude of 55 MPa (8 ksi) and frequency of 0.6 Hz. A positive stress amplitude of 0.1 MPa was used to avoid crack closure. Therefore, the value of the load ratio (R), which is calculated as the ratio between the minimum (σ_{min} = 0.1 MPa) and maximum (σ_{max} = 55 MPa) stress applied to the specimen, is close to 0. The σ_{max} is selected as it represents a maximum value observed in a typical miter gate based on finite element analysis. The lower load frequency (less than 1 Hz) is selected to ensure that the impact of the underwater environment is significant on the crack growth rate as discussed by Salivar et al. (1981). To apply these stresses to the tested specimens, a load control procedure is used. The maximum load (F) applied to the specimens is calculated as a function of the desired stresses on the crack plan (σ_{max} or σ_{min}) and the specimen cross section area at this location (A_{net}). The strain data are also used to verify the applied stresses on the tested specimens. Load commands were sent to the actuator using an MTS FlexTest controller. Force and displacement feedback were recorded by the controller. Strain data were recorded continuously throughout the tests using the data acquisition system.

At the beginning of each test, the initial crack was monitored closely to detect crack initiation. The initial crack length was taken as the out-to-out distance between the tack welds on either end of the cut crack. Crack propagation was taken to begin when a crack had initiated and grown through the tack welds. Crack length was then measured manually to the nearest 1.5 mm (1/16 in.) in regular increments for the test duration.

A dye penetrant was used when measuring crack lengths to clearly identify the crack tip. Dye penetrant is a visual inspection method for detecting flaws. Typically, the dye is applied to a surface and allowed to penetrate any flaws. Then the excess dye is wiped from the surface, and a developer is applied. The developer draws out dye remaining in the flaws, making their location appear clearly. In this case, the dye was applied during the fatigue loading, and the crack tip was identified by the dye forced out during the crack closure portion of the cycle.

For the retrofitted specimens, crack lengths were only measured when the crack tip was not beneath an FRP patch since no additional method for detecting the crack through the FRP was implemented. Visual observations of retrofit behavior were also made throughout the test to help identify any debonding behavior for comparison to that detected by the strain gauges along the length of the FRP patches.

Tests were considered complete when the crack length was such that final fracture of the specimen was imminent. Specimens were not intended to be tested to fracture because the fracture can cause a shock to the test frame, possibly altering alignment or affecting bolt pretension. Typically, the crack grew to 100 mm to 120 mm away from the specimen edge before crack growth accelerated dramatically and the test was stopped.

4 Experimental Results and Discussion

4.1 Introduction

Results from the eight tested specimens are presented and discussed herein. Each specimen was cyclically loaded as previously described until a fracture occurred or was imminent. Crack growth versus the number of cycles and strain in the steel and FRP, when applicable, were recorded throughout the tests. Comparison of specimens S1 and S2 allowed for the deleterious effect of the underwater environment to be quantified. The effectiveness of the retrofit methods was determined by comparison of the repaired specimens to the unrepaired specimens. Comparison of specimens S3 and S5 with specimens S4 and S6 allowed for assessment of the use of BFRP as an alternative to CFRP. The impact of the patch configuration was investigated by comparing the repaired specimens with two patches (specimens S2 to S6) with the repaired specimens with a full patch (specimens S7 and S8).

During each test, crack length was measured for the east and west cracks on both the north and south faces, and the average values for the east and west cracks were recorded each time that measurements were taken. The maximum strain values recorded during the times between the crack measurements process are utilized to compare the strain data in this section. For unretrofitted specimens, crack growth data were used to calculate Paris Law parameters C and m for use in future numerical analysis. Observations of the crack behavior were made for each specimen during and after the tests. After test completion, specimens that remained intact were cut along the crack plane in order to observe the characteristics of the crack face. In addition, the FRP bond was closely monitored for the retrofitted specimens. Debonding around the edges of the adhesive was detected. The failure mode of the FRP was observed at the end of tests of retrofitted specimens as either debonding failure, fiber rupture failure, or a combination. The galvanic corrosion was not directly measured during the test and the debonding around the edges was utilized as an indication of a possible galvanic effect. Details on the behavior of each specimen are noted below.

4.2 Specimens' Failure Mode

In comparison to fatigue in air, corrosion fatigue is more complex and requires the consideration of more variables such as load frequency and chemical properties of the water. Although the exact contributions to corrosion fatigue remain unclear due to difficulty in differentiating between all mechanisms during experimentation, hydrogen embrittlement and anodic dissolution are commonly attributed as the main driving factors (Salivar et al. 1981). Hydrogen embrittlement increases the crack growth rate by making the material around the crack more brittle. Hydrogen in water absorbs into crack surfaces and interferes with grain boundary cohesion. Anodic dissolution occurs as the newly exposed material from crack growth reacts with the water and is dissolved (Gangloff 2009). In the air, loading frequency has little effect on fatigue crack growth rate in steels. However, in underwater environments, frequency becomes an important factor due to the time dependence of the chemical reactions that contribute to increased growth rates.

In addition to hydrogen embrittlement impacting fatigue life, partial debonding, which occurred in some repaired specimens, had an impact on fatigue life. At the early stage of the tests prior to the cracks reaching the FRP patches, the growth rate of the cracks is lower for specimens retrofitted using CFRP as a result of the higher stiffness of the CFRP patches, which promoted crack closure. However, as the cracks continue to propagate, the high stiffness of the CFRP patches attracts larger forces, causing some debonding in the patches. On the other hand, the BFRP has lower stiffness, causing it to be less effective in closing the crack in the early stages of the propagation. However, the lower stiffness characteristic is beneficial overall in reducing stresses in the repairs and eliminating debonding.

For specimen S1, the west side of the crack exhibited stable growth until a half-crack length of approximately 300 mm at 975,000 cycles. The east side of the crack became unstable at a slightly lower crack length of approximately 250 mm at 990,000 cycles due to the uneven crack growth across the two sides. The test was stopped at 1,031,428 cycles when fracture of the west side was considered imminent to avoid damage to the test frame. Although fracture of the east side was not yet imminent, the east crack was showing unstable growth. The crack at the time of test completion is shown in Figure 18*a*.

For specimen S2 (underwater specimen), the crack growth was stable until a half-crack length of approximately 300 mm. Both cracks reached 300 mm after approximately 880,000 cycles. The test was stopped at 925,000 cycles, when the crack began to grow very rapidly and the fracture was imminent. Figure 18*b* shows specimen S2 after the test was completed and the specimen was removed from the testing frame.

Figure 18. Failure of the different specimens.

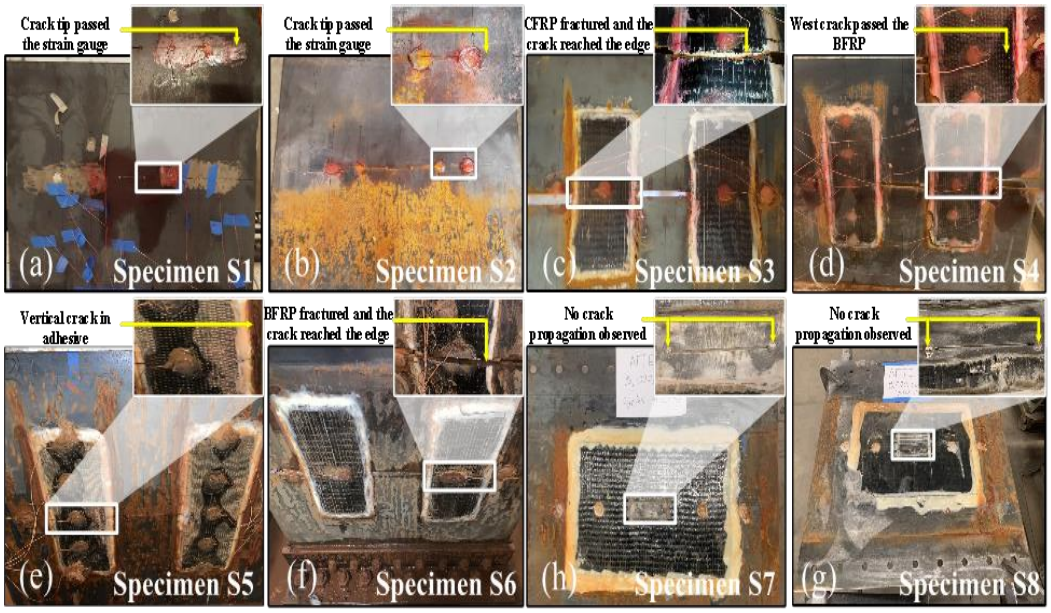

For specimen S3, the adhesive debonded around the crack tip on the north face of the west crack at approximately 415,000 cycles. Debonding was also noticed along the top boundary of the CFRP patches on the north side at 380,000 cycles. By 705,000 cycles, the debonding of both north patches had propagated down the top quarter of the inner edges of the patches. At 905,000 cycles, the inner edges of the north patches had debonded on the entire top half, and the outer edges had debonded on the top quarter. The edges of the entire top half of the north CFRP patches had debonded by 955,000 cycles, as shown in Figure 18*c*.

After 510,000 cycles, specimen S4 showed slight but not significant debonding directly adjacent to the cracks and began to propagate under the BFRP patches. At 1,680,100 cycles, the west crack, with a length of 275 mm, appeared beyond the BFRP patch. Once beyond the patch, the west crack grew quickly until it fractured at 1,765,458 cycles. as shown in Figure 18*d*. The east crack was not visible beyond the BFRP patch until the final

fracture of the west half, at which point it was approximately 20 mm beyond the adhesive fillet.

For specimen S5, a vertical crack on adhesive at the south side of the crack was visually noticed at 845,000 cycles. Debonding around the crack did not appear to propagate significantly along the vertical inside edges of the patches throughout the test. No visibly detectable debonding of the patch ends occurred throughout the entire test. At 1,295,000 cycles, the west crack appeared beyond the CFRP patch. Once beyond the patch, the west crack grew quickly until it fractured at 1,310,875 cycles, as shown in Figure 18*e*. The east crack was not visible beyond the CFRP patch until the final fracture of the west half.

For specimen S6, no significant debonding occurred during the test. However, at 1,750,000 cycles and due to the specimen's instability after the west crack appeared beyond the BFRP patch, the patches located on the lower part of the east crack debonded. Once beyond the patch, the west crack grew quickly until it fractured at 1,797,062 cycles, as shown in Figure 18*f*.

For specimens S7 and S8, the test stopped at 3 million cycles, and the patches were partially saw cut to expose the crack tip as shown in Figures 18*g* and 18*h*, respectively. It can be noticed from the figures that in both specimens the crack did not initiate, indicating an infinite life. From the observed failure modes for different specimens, it can be concluded that the fiber bonding was significantly enhanced compared with the previous study by Mahmoud et al. (2018), which was directly impacted by utilizing the glass fiber as isolation for the CFRP to reduce or prevent the galvanic corrosion and using BFRP, which does not cause galvanic corrosion.

Since the tests were conducted using a load control procedure, the degradation can be measured using the change (increase) in the measured displacement. Minor stiffness degradation of less than 1% over the test total number of cycles was noticed for all the tested specimens before the crack growth passed the patches or large deponding occurred. For specimens S7 and S8, no degradation was recorded. The axial stiffness for all the repaired specimens with two patches (S3 to S6) were higher than the unretrofitted specimen S2 by up to 2.2%. Due to the difference in the axial stiffness between the CFRP and BFRP, the measured axial stiffness for specimen S3 was 2.3% higher than for specimen S4. Due to the change

in the retrofitted sheet configuration, the axial stiffnesses for specimens S7 and S8 were higher than for specimens S5 and S6 by 7.2% and 5.8%, respectively.

4.3 Specimens' Fatigue Life

The fatigue life was used as the primary metric for comparing results across specimens and determining the effectiveness of the retrofits. As expected, all proposed retrofitting methods improved fatigue life, and the underwater environment reduced fatigue life in comparison to fatigue in air condition. Crack growth data for all specimens are shown in Figure 19. For all the specimens, the cracks initiated from the tack welds at both ends of the pre-cut crack at approximately the same time. The initial phase of crack propagation is affected by the presence of the tack welds on both sides of the introduced crack. The number of cycles measured before the crack grew past the tack welds was 87,173; 80,000; 92,000; 94,000; 90,000; and 96,000 for specimens S1 to S6, respectively. However, no initiation was recorded for specimens S7 and S8. The cycles associated with initiation caused by the tack welds were subtracted from the total number of cycles reported for each test.

Figure 19*a* shows that for specimen S1, the two crack tips propagated at similar rates until reaching a half crack length of 75 mm. After this point, the west crack began to propagate more quickly than the east crack. The difference in length between the two cracks increased throughout the test. However, at the completion of the test, the west crack was 100 mm longer than the east crack. Measurements of crack growth for specimen S2 are shown in Figure 19*b*. The two crack tips propagated at similar rates until reaching a half-crack length of 200 mm. After this point, the east crack began to propagate more quickly than the west crack. At the completion of the test, the east crack was 40 mm longer than the west crack.

For specimen S3, the west side of the crack immediately began to grow more quickly than the east side, as shown in Figure 19*c*. The width of the adhesive extending beyond the CFRP varied slightly at each location but was approximately 80 mm from the tack welds. The west crack reached a length of 93 mm at 380,000 cycles before reaching the adhesive. The east crack reached a length of 68 mm at 285,000 cycles and then could no longer be measured.

Figure 19. Comparison of crack growth and fatigue life for all specimens.

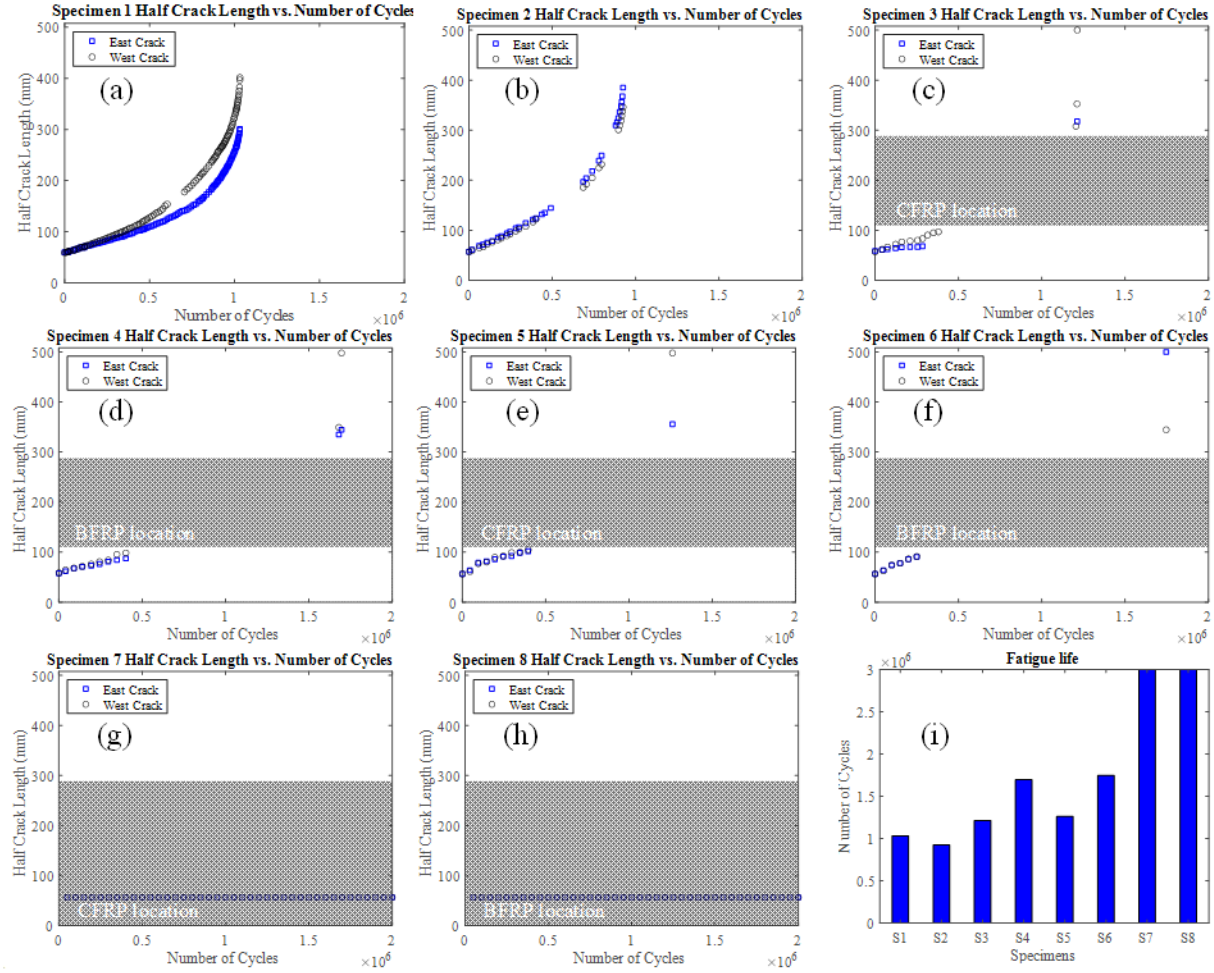

Cracks in specimen S4 began to propagate on both sides of the initial notches at the same time. Crack propagation results are shown in Figure 19*d*. The width of the adhesive extending beyond the BFRP varied slightly at each location. The length of the west crack was 98 mm at 402,000 cycles before reaching the adhesive. The east crack reached a length of 87 mm at 402,000 cycles and then could no longer be measured. The two crack tips for specimen S5 almost propagated at similar rates until reaching the adhesive at 395,000 cycles as displayed in Figure 19*e*. At the completion of the test, the west crack was 45 mm longer than the east crack.

For specimen S6, the two crack tips propagated at similar rates until reaching the adhesive at 245,000 cycles as shown in Figure 19*f*. At the completion of the test, the east crack was approximately 155 mm longer

than the west crack. The cracks in specimens S7 and S8 did not propagate as displayed in Figure 19*g* and *h*.

A comparison between the fatigue life of all the tested specimens is shown in Figure 19*i*. A freshwater environment reduced the fatigue life by more than 10.3%. Utilizing two patches of CFRP can enhance the fatigue life between 31.1% and 36.3% compared with unretrofitted specimens tested in the underwater environment. However, using BFRP and the same repair configuration can improve the fatigue life between 83.4% to 89.0% compared with unretrofitted specimens tested in the underwater environment. Eventually, employing full patches that cover the crack resulted in infinite fatigue life for the specimens. These increases in the fatigue life were significant compared with a previous study by Mahmoud et al. (2018), where the fatigue life was only increased by 16% by using one layer of the CFRP sheet without an insulation layer of the glass fiber layer. The increase in performance in this study compared with the previous study (Mahmoud et al. 2018) is due to the effectiveness of the glass fiber in insulating the CFRP and preventing galvanic corrosion, the significance of using two layers of FRP in reducing the stresses on the crack plane, and efficiency of the BFRP in reducing the crack growth.

To further reflect on the crack growth rate for the unrepaired specimens (in air and underwater,) the parameters for Paris' law were calculated from the test data. Paris' law can be applied as a simple analytical method for understanding the growth rate of the test specimens' crack. Using the crack growth data acquired from specimens S1 and S2, Paris' law parameters C and m were estimated by calculating crack growth rate (da/dN) and stress intensity factor range (ΔK). C and m are the y-intercept and slope, respectively, of da/dN versus ΔK plotted on a log-log scale, as shown in Figure 20. Separate parameters were calculated for the east and west cracks. The difference between the estimated parameters for the east and the west cracks is minimal, which could be due to uneven stress distribution in the specimen due to minute misalignment in the test setup. Calculated parameters are for crack length and stress intensity factor in units of mm and MPa-$mm^{1/2}$, respectively. The first several crack length measurements were excluded from the calculation because they may have been affected by the presence of the tack welds. Additionally, measurements taken after unstable growth was noted were excluded, as Paris' law no longer applies. A comparison between specimens S1, shown in Figure 20*a*, and specimen S2, displayed in Figure 20*b*, reveals that in

each specimen there was a difference between the crack growth rates for the east and west sides. The slope values for the east and west cracks, per meter, reduced from 2.51 and 1.58 for specimen S1 to 1.58 and 1.35 for specimen S2, which reflects the impact of the surrounding environment on the accelerating crack growth rates.

Figure 20. Plot of crack growth rate and stress intensity factor range for determination of Paris' law parameters for (*a*) specimen S1 and (*b*) specimen S2.

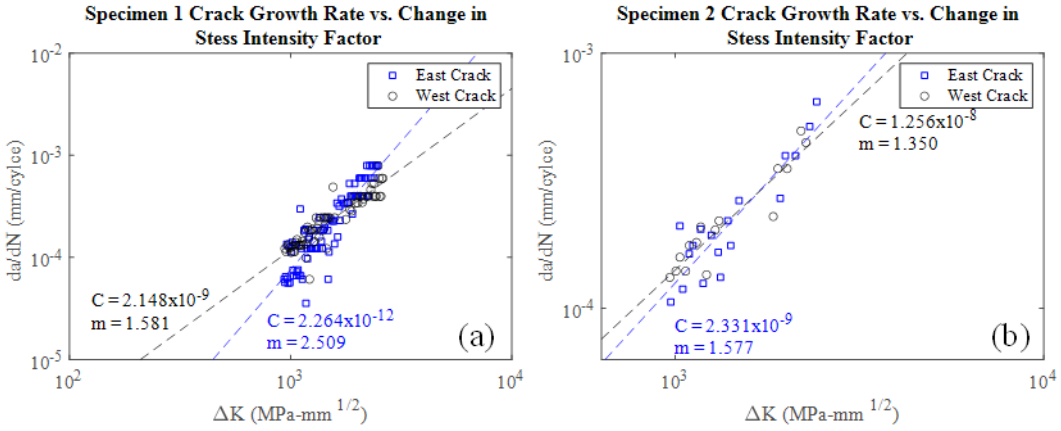

4.4 Specimens' Strains

Strain gauges applied on the steel were located along the crack plane, and readings corresponding to measured crack lengths are shown in Figure 21 for specimens S3, S4, S5, and S6 that were retrofitted with two patches. For specimen 3, the strain in gauges 1 and 4 located on the east side of the specimen increased as the crack approached the gauges. The crack did not reach the gauges, however, due to a fracture of the west side. This means that the maximum strain that would have occurred when the crack tip reached the gauges was not recorded. Strain gauges 2 and 3 located on the west side showed a slight increase as the crack approached, but no rapid increase in strain was noted. As the west crack grew, it curved slightly upward such that its path was above the strain gauges rather than directly through them, so elevated strain values were not observed. For specimen S4, a rapid increase in the readings from strain gauges 2 and 3 along the west was recorded after the crack length was beyond the BFRP. However, the elevated values were not as high as those recorded for other specimens because the crack grew slightly above the strain gauges.

Figure 21. Strain data from strain gauges located in the steel at the crack plane vs. half-crack length for specimens strengthened with two patches including (*a*) specimen S3, (*b*) specimen S4, (*c*) specimen S5, and (*d*) specimen S6.

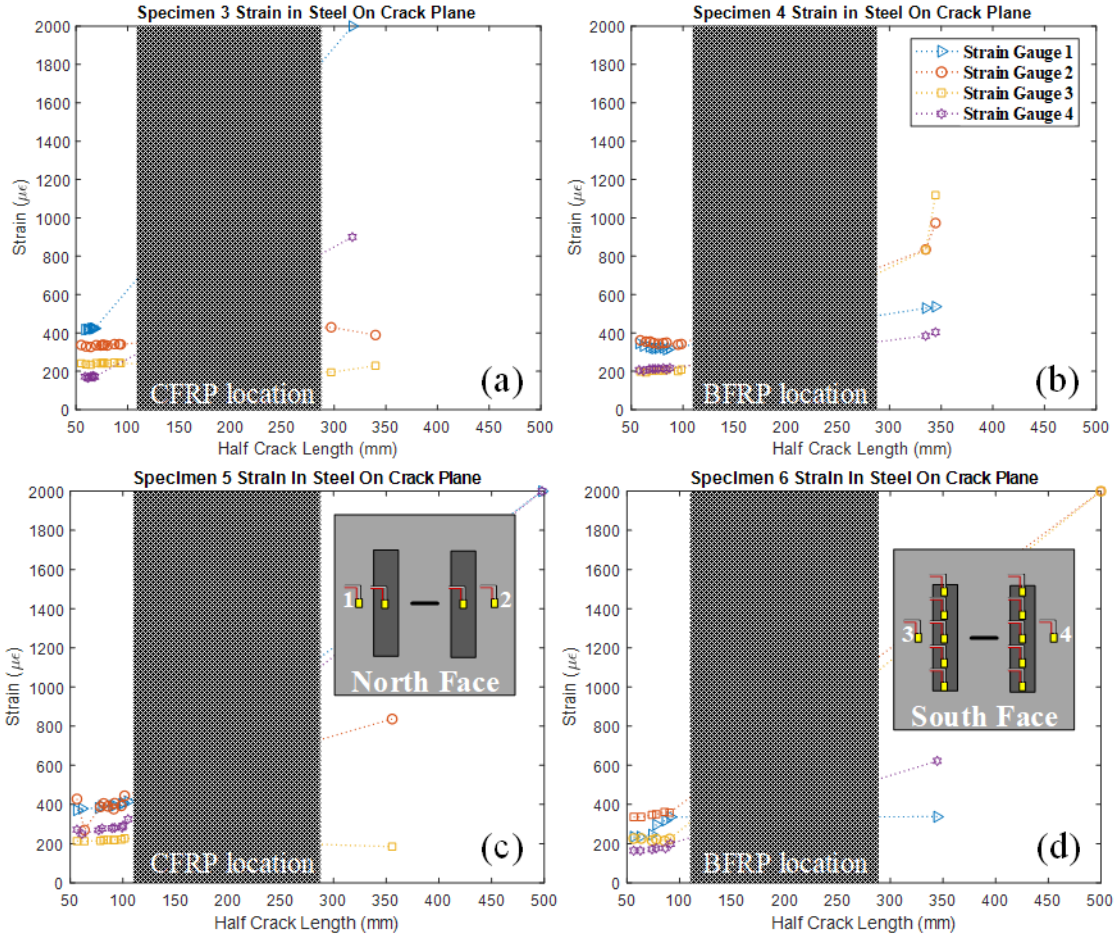

The east crack approached strain gauges 1 and 4 just as the fracture of the west half of the specimen took place, and increased values were recorded at that instance. For specimen S5, once the crack was beyond the CFRP, the readings from strain gauges 1, 2, and 4 were significantly increased. At the same time, the readings from strain gauge 3 were also increased but with less magnitude, which matched the observation that the crack grew past slightly above strain gauge 4 located in the east half before the west half of the specimen fractured. Unlike the previously retrofitted specimens, the fracture in specimen S6 occurred in the east half. Strain data for strain gauges 2 and 3 located in the east half showed a sudden increase in strain magnitude while increases recorded for strain gauges 1 and 4 were mild. The crack in the west half was about to approach strain gauges 1 and 4 in the same instance when the fracture of the west half took place.

Strain gauges on the FRP were installed along the crack plane on both faces and along the height of the patches on the south face. A comparison between the strain data collected from these strain gauges is shown in Figure 22. Similar to Figure 21, this figure displays the results of the specimens repaired with two patches. The strain magnitudes were non-uniformly distributed over the patches. For all the specimens, strain magnitudes recorded in the strain gauges located in the south face were less than the ones located in the north face. For specimen S3, Figure 22*a* shows that recorded values from strain gauges 5 and 6 slightly dropped during the test, which is an indication that debonding occurred in the patches located on the north face. All the strain gauges on the south face showed an increase in the strain magnitudes throughout the test, indicating that they remained well bonded. The south patches were bridging the crack and providing a crack closure effect until they ruptured. Unlike specimen S3, the magnitudes of all the strains were increasing with the half-crack length indicating that no debonding took place in specimens S4, S5, and S6 as shown in Figures 22*b*, 22*c*, and 22*d*, respectively.

Figure 22. Strain data from strain gauges located in the patches at the crack plane vs. half crack length for specimens strengthened with two patches including (*a*) specimen S3, (*b*) specimen S4, (*c*) specimen S5, and (*d*) specimen S6.

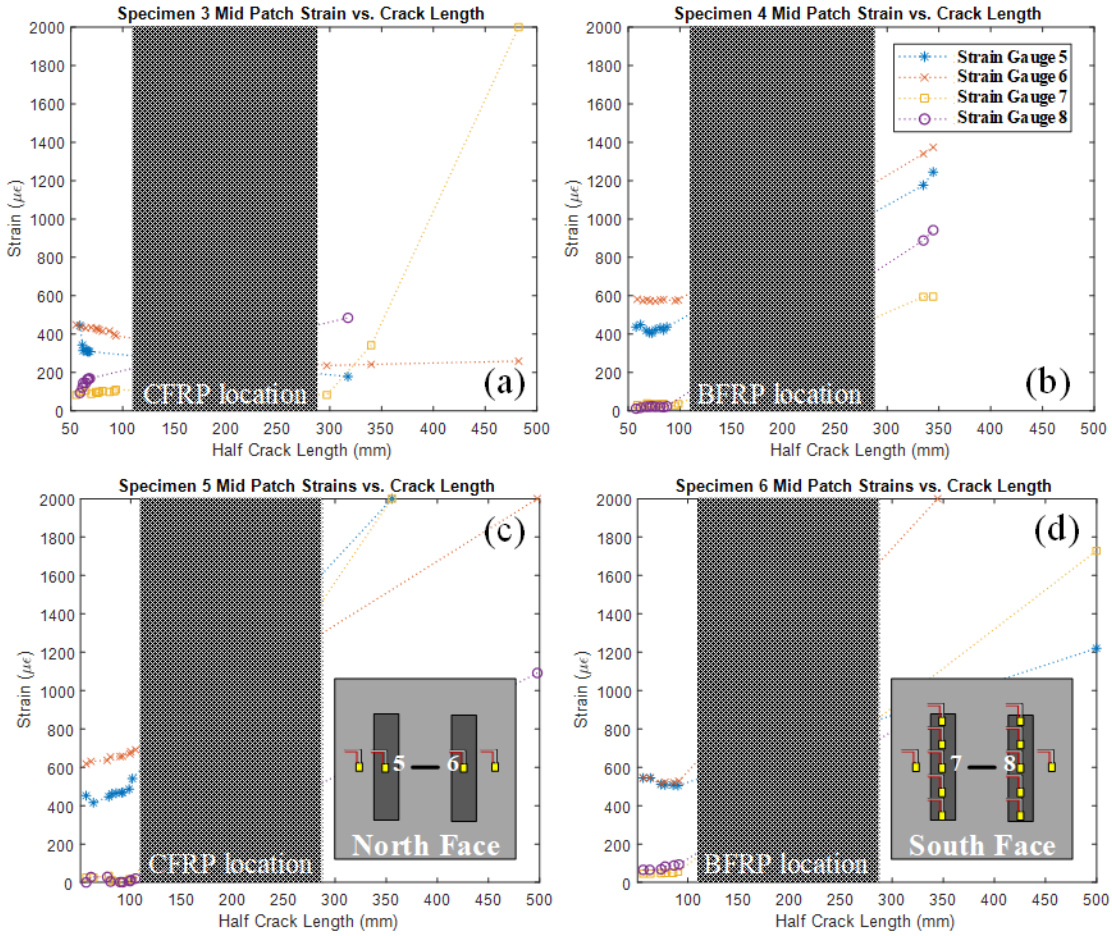

Strain gauges were also placed along the height of the patches on the south face to assist with detecting debonding from the steel. The strain results from the west half of the specimen are used as an example of the CFRP behavior and the strain distribution along the patches. Figures 23*a* and 23*b* show the strain data collected from specimens S3 and S4, respectively. For both specimens, all the strain gauges on the south face recorded increasing strains throughout the test, indicating that they remained well bonded. Therefore, the south patches were effectively bridging the crack and providing a crack closure effect until they ruptured. However, for specimen S3, only one of the strain gauges that was located on the north side of the specimen, shown in Figure 22*a*, showed decreasing values throughout the test. This matches the visual observation on that face.

Figure 23. Plot of the strain data collected from strain gauges located along the height of the repair patches in the south face and at the west half of the specimens (*a*) S3 and (*b*) S4.

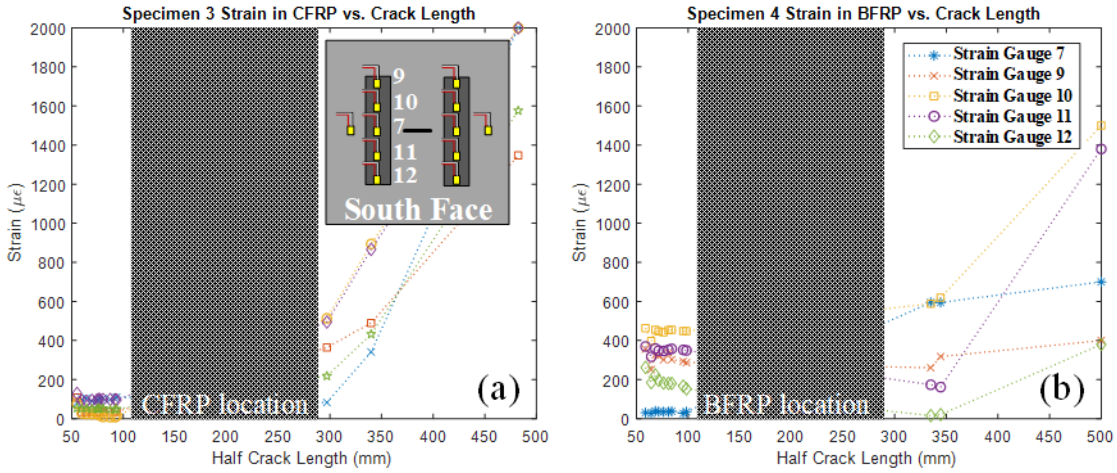

To understand the strain distribution on the crack plane for the specimens S7 and S8 which were repaired with full patches, five strain gauges are installed on each face of each specimen. The strain data for these two specimens were stable, and no changes in the strain were recorded over the test. A comparison between the values of the strain data collected from these strain gauges is displayed in Figures 24*a* and 24*b* for specimens S7 and S8, respectively.

The results show that the strain distributions on the north and south faces are slightly different, which was attributed to slight misalignment in the test frame. Variation in the strain distribution between the north and south faces for the specimen retrofitted with the BFRP was less compared with the specimen retrofitted with CFRP, which is an indication of the effectiveness of the BFRP in redistributing the strain and stresses over the tested specimen's components. Also, the average strains on the BFRP patches were less than on the CFRP patches. The average strains in the steel repaired with BFRP were more than the ones repaired with CFRP. The average strains recorded on the west and east sides of both were symmetric, where the average strains recorded at strain gauges 1 and 2 were similar in magnitude to the strains in strain gauges 4 and 5, respectively. This similarity in the recorded strains reflects the symmetry in the test configuration between the east and west sides. These two tests were stopped when the number of cycles reached the pre-defined threshold of 3 million cycles and the crack in these two specimens showed no initiation.

Figure 24. Plot of the strain data collected from strain gauges located along the crack length of the specimens (*a*) S7 and (*b*) S8.

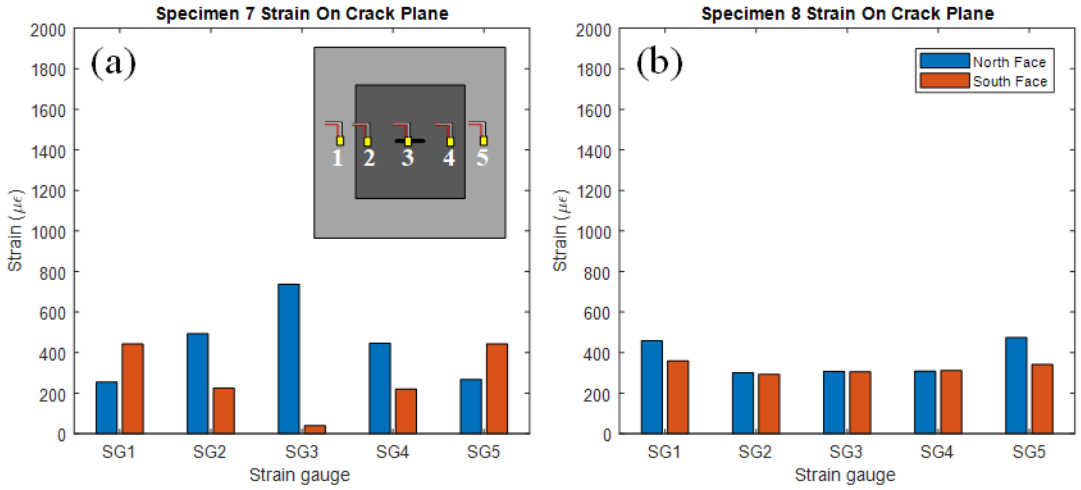

5 Conclusion

5.1 Summary of Current Work

Eight large-scale center-cracked tension specimens were fabricated for fatigue testing. Six of these specimens were retrofitted using bonded FRP patches and tested in an underwater environment and compared with unretrofitted specimens tested in an air and underwater environment. CFRP, which has previously been used in various studies for fatigue crack repair in steel, was used to retrofit one specimen. Another specimen was retrofitted with BFRP, which has very limited previous use in civil engineering applications but does not react galvanically with steel, which CFRP does. Two different configurations for the FRP patches were tested using either two separate patches or one full patch. Special consideration was given to the quality of the bond between the steel and FRP because several previous studies indicate that FRP retrofits are limited by the bond. An underwater environment was introduced for the retrofitted specimens and one unretrofitted specimen to simulate the environment experienced by steel hydraulic structures and evaluate whether the retrofit methods are suitable for that environment.

Constant amplitude mode I fatigue tests were carried out for each specimen. Crack growth and FRP behavior were monitored throughout the tests. Results from the two unretrofitted specimens, only one of which was tested underwater, were compared to identify the reduction in fatigue life due to an underwater environment. Results from the different, retrofitted, and unretrofitted, specimens were compared to identify the enhancement in fatigue life due to different environments, various FRP types, and a variety of the FRP configurations. The use of BFRP as an alternative to CFRP was evaluated by comparing the two retrofitted specimens.

5.2 Conclusions

Results from the unretrofitted specimens tested in air and water confirmed that crack growth accelerates underwater; a decrease in fatigue life of 10.3% was recorded when tested in an underwater environment. Although fatigue life was not reduced tremendously, the effect of the underwater environment can become substantial throughout the long service life.

The retrofit methods using two patches of both CFRP and BFRP were shown to be viable for increasing fatigue life of a center-cracked panel with increases over the underwater unretrofitted specimen of 36.3% and 89.0% for CFRP and BFRP, respectively.

CFRP performance was enhanced in this experiment testing compared with previously published studies as a result of using glass fiber as an insulating layer and proper application process, which highlights the need for the installation procedures when using the CFRP as a retrofit material in an underwater environment.

BFRP over performed the CFRP due to its ability to avoid galvanic corrosion, enhance the durability in the underwater environment, and reduce the demand on the adhesive. Even though the sample size was small, the positive results of the BFRP specimens showed promise that the BFRP can be the future repair of fatigue damage in steel, especially in an underwater environment.

The higher stiffness of the CFRP was apparent when comparing crack growth and strain distribution with BFRP before the cracks reached the FRP patches. BFRP was also effective in the redistribution of the stresses over the tested specimens' components.

The retrofitting configuration utilized has a significant impact on the expected fatigue life of the center-cracked panels. The results showed that using a single patch that covers the center crack can assure an infinite fatigue life of the tested specimen. It can also significantly reduce the stresses on the crack tip and delay the crack opening.

The results show that the use of glass fiber as an insulation layer between the CFRP and the steel and the use of BFRP to repair the steel structures subjected to high-cycle fatigue and submerged in the freshwater environment can significantly enhance fatigue life. While these findings are applicable to underwater cracked steel elements subjected to mode I fatigue loading and fabricated using different structural steel grades (ANSI/AISC 360-16 2016), the impact of the element's exposure time to the harsh surrounding environment on the repair effectiveness needs further investigation.

5.3 Recommendations for Future Work

Although the completed tests indicate that both CFRP and BFRP are viable repair options, the mechanisms caused by the underwater environment remain unclear. The extent to which saturation affected the adhesive properties and therefore contributed to the debonding in the specimen with CFRP is not known. Smaller scale testing to isolate the adhesive properties after water saturation is recommended. Exploring saturation over a longer time period is also recommended because time frame of the present tests was much shorter than the life span of a steel hydraulic structure. Since it is known that a threshold stress under which FRP will not debond exists, underwater bond fatigue tests for the FRP materials used would be useful for selecting future retrofit configurations. Additionally, the behavior of BFRP in both air and water is not well understood due to its limited prior use. Should BFRP be selected for further use, material properties, fatigue strength, and underwater durability should be tested on a small scale.

Based on the current results and the methods previously used by others, the following modifications for improving the retrofit method are recommended if additional large-scale tests of the same nature are performed:

- Develop a mechanical clamping method to apply confining pressure to the FRP patch ends and reduce debonding.
- Apply a sealant coating to the FRP patches to reduce exposure of the epoxies to water.

Extending the large-scale testing method to account for multimode loading or more complex geometry of the fatigue-damaged component would also provide additional insight for future field use because many locations in SHS that experience fatigue damage are more complex than the configuration tested in the current work.

Since it is not feasible to conduct large-scale testing for all field application configurations, a method for predicting remaining fatigue life after a crack is repaired is desirable. Both numerical and analytical methods for predicting crack growth in air after applying FRP repairs exist, but for the purpose of rapidly assessing a needed repair, a quick analytical approach would be more appropriate. An adaptation of the existing analytical models for growth of a repaired crack that accounts for the nominal stress

reduction and crack closure effects of the FRP is suggested. Results from this study and any additional experimental work may be useful for making empirical modifications to account for underwater environmental factors.

References

Al Azzawi, M., P. Hopkins, G. Mullins, and R. Sen. 2018. "FRP–Concrete Bond after 12-Year Exposure in Tidal Waters." *Journal of Composites for Construction* 22 (5): 04018031. https://doi.org/10.1061/(asce)cc.1943-5614.0000864.

ANSI/AISC. 2016. *ANSI/AISC 360-16*: *Specification for Structural Steel Buildings*. Chicago: ANSI/AISC.

Bocciarelli, M., P. Colombi, G. Fava, and C. Poggi. 2009. "Fatigue Performance of Tensile Steel Members Strengthened with CFRP Plates." *Composite Structures* 87 (4): 334–43. https://doi.org/10.1016/j.compstruct.2008.02.004.

Colombi, P. 2004. "On the Evaluation of Compliance Information for Common Crack Growth Specimens Reinforced by Composite Patch." *International Journal of Fracture* 125: 73–87. https://doi.org/10.1023/B:FRAC.0000021043.74064.1a.

Colombi, P., A. Bassetti, and A. Nussbaumer. 2003. "Crack Growth Induced Delamination on Steel Members Reinforced by Prestressed Composite Patch." *Fatigue and Fracture of Engineering Materials and Structures* 26 (5): 429–438. https://doi.org/10.1046/j.1460-2695.2003.00642.x.

Colombi, P., and G. Fava. 2015. "Experimental Study on the Fatigue Behaviour of Cracked Steel Beams Repaired with CFRP Plates." *Engineering Fracture Mechanics* 145: 128–42. https://doi.org/10.1016/j.engfracmech.2015.04.009.

Deng, J., and M. M. K. Lee. 2007. "Fatigue Performance of Metallic Beam Strengthened with a Bonded CFRP Plate." Composite Structures 78 (2): 222–31. https://doi.org/10.1016/j.compstruct.2005.09.003.

Dexter, R., H. N. Mahmoud, and P. J. Pilarski. 2005. "Propagation of Long Cracks in Stiffened Box-Sections under Bending and Stiffened Single Panels under Axial Tension." *International Journal of Steel Structures* 5 (3): 181–88.

Dexter, R., P. J. Pilarski, and H. N. Mahmoud. 2003. "Analysis of Crack Propagation in Welded Stiffened Panels." *International Journal of Fatigue* 25 (9–11): 1169–74. https://doi.org/10.1016/j.ijfatigue.2003.08.006.

Dorigato, A., and A. Pegoretti. 2012. "Fatigue Resistance of Basalt Fibers-Reinforced Laminates." *Journal of Composite Materials* 46 (15): 1773–85. https://doi.org/10.1177/0021998311425620.

Gangel, R. E. 2011. *Use of CFRP Overlays to Repair Fatigue Damage in Steel Bridge Giders and Components*. Lawrence, KS: University of Kansas.

Gangloff, R. 2009. "Environmental Cracking-Corrosion Fatigue." In R. Baboian (ed.), *Corrosion Tests and Standards: Application and Interpretation—Second Edition*. West Conshohocken, PA: ASTM International. https://doi.org/10.1520/mnl11032m.

Headquarters, US Army Corps of Engineers. 2010. Advanced reliability analysis of fatigue cracking in horizontally framed miter gates. ETL-1110-2-566. Washington, DC: Headquarters, U.S. Army Corps of Engineers.

Hollaway, L. C., and J. Cadei. 2002. "Progress in the Technique of Upgrading Metallic Structures with Advanced Polymer Composites." *Progress in Structural Engineering and Materials* 4 (2): 131–48. https://doi.org/10.1002/pse.112.

Jayasuriya, S., A. Bastani, S. Kenno, T. Bolisetti, and S. Das. 2018. "Rehabilitation of Corroded Steel Beams Using BFRP Fabric." *Structures* 15 (March): 152–61. https://doi.org/10.1016/j.istruc.2018.06.006.

Jones, S. C., and S. A. Civjan. 2003. "Application of Fiber Reinforced Polymer Overlays to Extend Steel Fatigue Life." *Journal of Composites for Construction* 7 (4): 331–38. https://doi.org/10.1061/(asce)1090-0268(2003)7:4(331).

Kang, D. H., J. K. Lee, and T. W. Kim. 2011. "Corrosion Fatigue Crack Propagation of High-Strength Steel HSB800 in a Seawater Environment." *Procedia Engineering* 10: 1170–75. https://doi.org/10.1016/j.proeng.2011.04.195.

Liu, F. T., G. H. He, and J. H. Xiong. 2017. "Experimental Study on Durability of FRP Sheets under Wet-Dry Cycles in Various Solutions." *Procedia Engineering* 210: 61–70. https://doi.org/10.1016/j.proeng.2017.11.049.

Liu, H., R. Al-Mahaidi, and X.-L. Zhao. 2009*a*. "Experimental Study of Fatigue Crack Growth Behaviour in Adhesively Reinforced Steel Structures." *Composite Structures* 90: 12–20. https://doi.org/10.1016/j.compstruct.2009.02.016.

Liu, H., X. L. Zhao, and R. Al-Mahaidi. 2005. "The Effect of Fatigue Loading on Bond Strength of CFRP Bonded Steel Plate Joints." In J. F. Chen and J. G. Teng (eds.), *Proceedings of the International Symposium on Bond Behaviour of FRP in Structures* (March): 451–56. The Hong Kong Polytechnic University.

Liu, H., X. Zhao, R. Al-Mahaidi, and S. Rizkalla. 2007. "Analytical Bond Models between Steel and Normal Modulus CFRP." *Fourth International Conference on Advances in Steel Structures* II: 1545–52. https://doi.org/10.1016/b978-008044637-0/50230-4.

Liu, H., Z. Xiao, X.-L. Zhao, and R. Al-Mahaidi. 2009*b*. "Prediction of Fatigue Life for CFRP-Strengthened Steel Plates." *Thin-Walled Structures* 47 (10): 1069–77. https://doi.org/10.1016/j.tws.2008.10.011.

Long, M., C. Djelal, S. Kesteloot, B. Bigourdan, P. Y. Le Gac, and J. Szulc. 2012. *Durability of Cfrp-Concrete Bonding in a Marine Environment* (June): 24–28.

Lozano, C. M., and G. A. Riveros. 2019. "Effects of Adhesive Bond-Slip Behavior on the Capacity of Innovative FRP Retrofits for Fatigue and Fracture Repair of Hydraulic Steel Structures." *Materials* 12 (9). https://doi.org/10.3390/ma12091495.

Mahmoud, H., A. Chulahwat, and G. Riveros. 2018. "Fatigue and Fracture Life-Cycle Cost Assessment of a Miter Gate with Multiple Cracks." *Engineering Failure Analysis* 83 (September): 57–74. https://doi.org/10.1016/j.engfailanal.2017.09.008.

Mahmoud, H. N., A. Como, and G. A. Riveros. 2014. *Fatigue Assessment of Underwater CFRP-Repaired Steel Panels Using Finite Element Analysis*. Technical Report ERDC-ITL TR-14-3. Retrieved from https://hdl.handle.net/11681/10828.

Mahmoud, H. N., and R. J. Dexter. 2005. "Propagation Rate of Large Cracks in Stiffened Panels under Tension Loading. *Marine Structures* 18 (3): 265–88. https://doi.org/10.1016/j.marstruc.2005.09.001.

Mahmoud, H., and G. Riveros. 2014. "Fatigue Reliability of a Single Stiffened Ship Hull Panel." *Engineering Structures* 66: 89–99. https://doi.org/10.1016/j.engstruct.2014.02.007.

Mahmoud, H. N., and G. A. Riveros. 2013. Fatigue Repair of Steel Hydraulic Structures (SHS) Using Carbon Fiber Reinforced Polymers (CFRP): Feasibility Study. Technical Report ERDC-ITL TR-13-1. https://erdc-library.erdc.dren.mil/jspui/bitstream/11681/10929/1/ERDC-ITL-TR-13-1.pdf.

Mahmoud, H. N., G. A. Riveros, M. Memari, A. Valsangkar, and B. Ahmadi. 2018. "Underwater Large-Scale Experimental Fatigue Assessment of CFRP-Retrofitted Steel Panels." *Journal of Structural Engineering* 144 (10): 04018183. https://doi.org/10.1061/(asce)st.1943-541x.0002184.

Matta, F.,V. M. Karbhari, and R. Vitaliani. 2005. "Tensile Response of Steel/CFRP Adhesive Bonds for the Rehabilitation of Civil Structures." *Structural Engineering and Mechanics* 20 (5): 589–608. https://doi.org/10.12989/sem.2005.20.5.589.

Mertz, D. R., J. W. Gillespie, M. J. Chajes, and S. A. Sabo. 2002. "The Rehabilitation of Steel Bridge Girders Using Advanced Composite Materials." In *NCHRP-IDEA Program Project Final Report*.

Misawa, T., and Y. Kobayashi. 1976. "Effect of pH on Corrosion Fatigue Crack Propagation in a Low Carbon Steel." *Corrosion Engineering* 25 (8): 493–97. https://doi.org/10.3323/jcorr1974.25.8_493.

Monfared, A., K. Soudki, and S. Walbridge. 2008. "CFRP Reinforcing to Extend the Fatigue Lives of Steel Structures." Fourth International Conference on FRP Composites in Civil Engineering (CICE2008), Zurich, Switzerland, 22–24.

Morgantini, M., V. Okorokov, Y. Gorash, D. Mackenzie, and R. Van Rijswick. 2018. "The Effect of Fresh Water Solution on Fatigue Strength of Low Carbon Steel" Lisbon, Portugal: 6th International Conference Integrity-Reliability-Failure (IRF2018), 289–296.

Nozaka, K., C. K. Shield, and J. F. Hajjar. 2005. "Effective Bond Length of Carbon-Fiber-Reinforced Polymer Strips Bonded to Fatigued Steel Bridge I-Girders." *Journal of Bridge Engineering* 10 (2): 195–205. https://doi.org/10.1061/(asce)1084-0702(2005)10:2(195).

Riveros, G. A., H. Mahmoud, and C. M. Lozano. 2018. "Fatigue Repair of Underwater Navigation Steel Structures Using Carbon Fiber Reinforced Polymer (CFRP)." *Engineering Structures* 173 (July): 718–28. https://doi.org/10.1016/j.engstruct.2018.07.016.

Riveros, G. A., H. Mahmoud, M. Memari, C. Lozano, A. Valsangkar, and B. Ahmadi. 2019. *Underwater Fatigue Repair of Steel Panels Using Carbon Fiber Reinforced Polymers*. Technical Report ERDC-ITL TR-19-1. https://doi.org/10.13140/RG.2.2.21236.30081.

Salivar, G. C., D. L. Creighton, and D. W. Hoeppner. 1981. "Effect of Frequency and Environment on Fatigue-Crack Propagation of SA533B-1 Steel." *Engineering Fracture Mechanics* 14: 337–52.

Shield, C., K. Nozaka, and J. Hajjar. 2004. *Repair of Fatigued Steel Bridge Girders with Carbon Fiber Strips*. Minneapolis: Minnesota Department of Transportation. Retrieved from https://hdl.handle.net/11299/771.

Tavakkolizadeh, M., and H. Saadatmanesh. 2001. "Galvanic Corrosion of Carbon and Steel." *Journal of Composites for Construction* 5 (August): 200–210.

Tavakkolizadeh, M., and H. Saadatmanesh. 2003. "Fatigue Strength of Steel Girders Strengthened with Carbon Fiber Reinforced Polymer Patch." *Journal of Structural Engineering* 129 (2): 186–196. https://doi.org/10.1061/(asce)0733-9445(2003)129:2(186).

Wu, C., X. Zhao, R. Al-Mahaidi, M. R. Emdad, and W. Duan. 2012. "Fatigue Tests of Cracked Steel Plates Strengthened with UHM CFRP Plates." *Advances in Structural Engineering* 15 (10): 1801–15. https://doi.org/10.1260/1369-4332.15.10.1801.

Wu, C., X.-L. Zhao, R. Al-Mahaidi, and W. H. Duan. 2013. "Effects of CFRP Bond Locations on the Mode I Stress Intensity Factor of Centre-Cracked Tensile Steel Plates." Fatigue and Fracture of Engineering Materials and Structures 36 (2): 154–67. https://doi.org/10.1111/j.1460-2695.2012.01708.x.

Wu, G., H.-T. Wang, Z.-S. Wu, H.-Y. Liu, and Y. Ren. 2012. "Experimental Study on the Fatigue Behavior of Steel Beams Strengthened with Different Fiber-Reinforced Composite Plates." *Journal of Composites for Construction* 16 (2): 127–37. https://doi.org/10.1061/(ASCE)CC.1943-5614.

Wu, Z., X. Wang, K. Iwashita, T. Sasaki, and Y. Hamaguchi. 2010. "Tensile Fatigue Behaviour of FRP and Hybrid FRP Sheets. *Composites Part B: Engineering* 41 (5): 396–402. https://doi.org/10.1016/j.compositesb.2010.02.001.

Zhao, X. L., and L. Zhang. 2007. "State-of-the-Art Review on FRP Strengthened Steel Structures." *Engineering Structures* 29 (8): 1808–23. https://doi.org/10.1016/j.engstruct.2006.10.006.

Zheng, Y., L. Ye, and X. Lu. 2006. "Experimental Study on Fatigue Behavior of Tensile Steel Plates Strengthened with CFRP Plates." Miami, FL: Third International Conference on FRP Composites in Civil Engineering (CICE), 5.

REPORT DOCUMENTATION PAGE

Form Approved

OMB No. 0704-0188

Public reporting burden for this collection of information is estimated to average 1 hour per response, including the time for reviewing instructions, searching existing data sources, gathering and maintaining the data needed, and completing and reviewing this collection of information. Send comments regarding this burden estimate or any other aspect of this collection of information, including suggestions for reducing this burden to Department of Defense, Washington Headquarters Services, Directorate for Information Operations and Reports (0704-0188), 1215 Jefferson Davis Highway, Suite 1204, Arlington, VA 22202-4302. Respondents should be aware that notwithstanding any other provision of law, no person shall be subject to any penalty for failing to comply with a collection of information if it does not display a currently valid OMB control number. PLEASE DO NOT RETURN YOUR FORM TO THE ABOVE ADDRESS.

1. REPORT DATE (DD-MM-YYYY)	2. REPORT TYPE	3. DATES COVERED (From - To)
03-2023	Final Report	

4. TITLE AND SUBTITLE

Experimental Fatigue Evaluation of Underwater Steel Panels Retrofitted with Fiber Polymers

5a. CONTRACT NUMBER

5b. GRANT NUMBER

5c. PROGRAM ELEMENT

6. AUTHOR(S)

Hussam N. Mahmoud, Guillermo Riveros, Lauren Hudak, and Emad M. Hassan

5d. PROJECT NUMBER

5e. TASK NUMBER

5f. WORK UNIT NUMBER

7. PERFORMING ORGANIZATION NAME(S) AND ADDRESS(ES)

U.S. Army Engineer Research and Development Center (ERDC)
Information Technology Laboratory (ITL)
3909 Halls Ferry Road
Vicksburg, MS 39180-6199

8. PERFORMING ORGANIZATION REPORT NUMBER

ERDC/ITL TR-23-1

9. SPONSORING / MONITORING AGENCY NAME(S) AND ADDRESS(ES)

Headquarters, US Army Corps of Engineers
Washington, DC 20314-1000

10. SPONSOR/MONITOR'S ACRONYM(S)

USACE

11. SPONSOR/MONITOR'S REPORT NUMBER(S)

12. DISTRIBUTION / AVAILABILITY STATEMENT

DISTRIBUTION A: Approved for public release; distribution is unlimited.

13. SUPPLEMENTARY NOTES

Navigation System Research Program, Work Unit DB5531, Funding Account Code U4376568, AMSCO Code 031391

14. ABSTRACT

Many steel structures are susceptible to fatigue loading and damage that potentially threaten their integrity. Steel hydraulic structures (SHS) experience fatigue loading during operation and exposure to harsh environmental conditions that can further reduce fatigue life through stress corrosion cracking and corrosion fatigue, for example. Dewatering to complete inspections or repairs to SHS is time consuming and leads to economic losses, and current repair methods, such as rewelding, often cause new cracks to form after relatively few cycles, requiring repeated inspection and repair. The use of bonded carbon fiber reinforced polymer (CFRP) to repair fatigue cracks in metallic structures has been successful in other industries; recent work suggests that this method offers a more reliable repair method for SHS.

Studies regarding CFRP retrofits of SHS indicate that early bond failure often controls the degree of fatigue life extension provided by the repair. This study aims to extend previous studies and increase the fatigue life of repaired steel components by employing methods to improve CFRP bonding. Additionally, using basalt reinforced polymer (BFRP) instead of CFRP is proposed. BFRP is attractive for SHS because it does not react galvanically and has excellent resistance to chemically active environments.

15. SUBJECT TERMS

Hydraulic stuctures--Maintenance and repair; Service life (Engineering); Underwater construction; Steel, Structural--Fatigue--Cracking; Carbon fiber-reinforced plastics

16. SECURITY CLASSIFICATION OF:			17. LIMITATION OF ABSTRACT	18. NUMBER OF PAGES	19a. NAME OF RESPONSIBLE PERSON
a. REPORT	b. ABSTRACT	c. THIS PAGE			19b. TELEPHONE NUMBER (include area code)
Unclassified	Unclassified	Unclassified	None	62	